

# Pharmacological target-focused transcriptomic analysis of native vs cultured human and mouse dorsal root ganglia

Andi Wangzhou<sup>a</sup>, Lisa A. McIlvried<sup>b</sup>, Candler Paige<sup>a</sup>, Paulino Barragan-Iglesias<sup>a</sup>, Stephanie Shiers<sup>a</sup>, Ayesha Ahmad<sup>a</sup>, Carolyn A. Guzman<sup>a</sup>, Gregory Dussor<sup>a</sup>, Pradipta R. Ray<sup>a,\*</sup>, Robert W. Gereau IV<sup>b</sup>, Theodore J. Price<sup>a</sup>

## Abstract

Dorsal root ganglion (DRG) neurons detect sensory inputs and are crucial for pain processing. They are often studied in vitro as dissociated cell cultures with the assumption that this reasonably represents in vivo conditions. However, to the best of our knowledge, no study has directly compared genome-wide transcriptomes of DRG tissue in vivo versus in vitro or between laboratories and culturing protocols. Comparing RNA sequencing-based transcriptomes of native to cultured (4 days in vitro) human or mouse DRG, we found that the overall expression levels of many ion channels and G-protein-coupled receptors specifically expressed in neurons are markedly lower although still expressed in culture. This suggests that most pharmacological targets expressed in vivo are present under the condition of dissociated cell culture, but with changes in expression levels. The reduced relative expression for neuronal genes in human DRG cultures is likely accounted for by increased expression of genes in fibroblast-like and other proliferating cells, consistent with their mitotic status in these cultures. We found that the expression of a subset of genes typically expressed in neurons increased in human and mouse DRG cultures relative to the intact ganglion, including genes associated with nerve injury or inflammation in preclinical models such as *BDNF*, *MMP9*, *GAL*, and *ATF3*. We also found a striking upregulation of a number of inflammation-associated genes in DRG cultures, although many were different between mouse and human. Our findings suggest an injury-like phenotype in DRG cultures that has important implications for the use of this model system for pain drug discovery.

**Keywords:** DRG, RNA sequencing, Pharmacology, Mrg receptors, Ion channels, GPCR, Receptor tyrosine kinase, DRG transcriptomics, DRG culture

## 1. Introduction

Nociceptors within the dorsal root ganglia (DRG) or trigeminal ganglia are the first neurons in the pain pathway.<sup>67</sup> These neurons are crucial contributors to chronic pain disorders ranging from inflammatory to neuropathic pain.<sup>3</sup> These neurons are frequently studied to gain insight into mechanisms that drive chronic pain and to develop better treatment strategies. Traditionally, investigators have studied rodent nociceptors in vitro as dissociated cell cultures prepared from DRG or trigeminal ganglia. More recently, investigators have also started to study DRG nociceptors from human organ donors and surgical patients.<sup>16,43,51,53,54,62,76</sup> This creates

a “clinical bridge” for advancing mechanisms or therapeutics from rodents toward the clinic. These models have many advantages; cultures can easily be used for electrophysiology, Ca<sup>2+</sup> imaging, biochemical, or other functional studies. These studies have unquestionably advanced the field of pain neurobiology and sensory transduction.

Despite the widespread use of this model system,<sup>38</sup> many investigators are skeptical of the degree to which these cells in dissociated culture accurately reflect the status of nociceptors in vivo. Several studies have analyzed the genome-wide RNA profiles of these dissociated cultures,<sup>26,47</sup> but not in the context of changes with respect to the native, acutely dissected ganglia (referred to as “intact” DRG henceforth). A previous study by Thakur et al.<sup>57</sup> contrasted RNA sequencing (RNA-seq) profiles of intact DRG with unsorted, acutely dissociated DRG. The study found few differences between intact DRG tissue and unsorted, acutely dissociated DRG, suggesting that the process of dissociation does not dramatically alter the molecular phenotype. Although some studies have compared expression of a single gene or a handful of genes in these in vitro cultures vs the intact ganglia,<sup>23,53</sup> we are unaware of any study that has used genome-wide assays to study how gene expression might be altered from native to cultured DRG conditions. We addressed this question by comparing intact vs cultured DRG from human donors and mice using RNA-seq. We designed a series of experiments to study how the transcriptomes of human and mouse native DRG differ under the conditions of dissociated cell cultures relative to

Sponsorships or competing interests that may be relevant to content are disclosed at the end of this article.

<sup>a</sup> School of Behavioral and Brain Sciences, Center for Advanced Pain Studies, The University of Texas at Dallas, Richardson, TX, United States, <sup>b</sup> Department of Anesthesiology, Washington University Pain Center, Washington University School of Medicine, St. Louis, MO, United States

\*Corresponding author. School of Behavioral and Brain Sciences, BSB14, The University of Texas at Dallas, Richardson TX 75080, United States. Address: E-mail address: prr105020@utdallas.edu (P.R. Ray).

Supplemental digital content is available for this article. Direct URL citations appear in the printed text and are provided in the HTML and PDF versions of this article on the journal's Web site ([www.painjournalonline.com](http://www.painjournalonline.com)).

PAIN 161 (2020) 1497–1517

© 2020 International Association for the Study of Pain

<http://dx.doi.org/10.1097/j.pain.0000000000001866>

native, intact ganglia. Our findings provide a comprehensive, genome-wide evaluation of gene expression changes from native to cultured DRG in both humans and mice. Consistent with previous studies,<sup>19,44</sup> we found that DRG neurons in culture show transcriptional signatures that suggest an injury phenotype.<sup>6,27</sup> This supports the use of cultured DRG neurons as a model system to study underlying mechanisms of pain. However, our findings point out some shortcomings of using these models to study multiple classes of receptors that show altered expression in culture. Some of these differences do not occur consistently across species, suggesting mouse DRG cultures may not be a good surrogate for human cultures in certain experiments. The data provided in this study will help investigators choose and design appropriate experimental parameters and can provide an important tool for future experiments in the pain and somatosensory fields.

## 2. Methods

### 2.1. Experimental design

Because genetic variation can be a possible contributor to transcriptome level differences in nervous system samples from human populations,<sup>43,45</sup> we chose a study design wherein we cultured lumbar DRG from one side in human donors and immediately froze the opposite side from the same donor for RNA sequencing. Although we used an inbred mouse strain (C57BL/6) for parallel mouse studies, we used a similar culturing design where cultures were performed in 2 independent laboratories to look for variability across laboratories. RNA sequencing was performed at 4 days in vitro (DIV) to stay within the electrophysiologically relevant range of 1 to 7 DIV for human DRG and the biochemical assay range of 4 to 7 DIV for both human and mouse DRG.

### 2.2. Animals

#### 2.2.1. Price laboratory

All procedures were approved by the Institutional Animal Care and Use Committee of University of Texas at Dallas and were in strict accordance with the US *National Institute of Health (NIH) Guide for the Care and Use of Laboratory Animals*. Adult C57BL/6 mice (8–15 weeks of age) were bred in house and were originally obtained from The Jackson Laboratory. Animals were housed in the University of Texas at Dallas animal facilities on a 12-hour light/dark cycle with access ad libitum to food and water.

#### 2.2.2. Gereau laboratory

All procedures were approved by the Animal Care and Use Committee of Washington University and in strict accordance with the US *National Institute of Health (NIH) Guide for the Care and Use of Laboratory Animals*. Adult C57BL/6 mice (8–15 weeks of age) were bred in house, originally obtained from The Jackson Laboratory. Animals were housed in Washington University School of Medicine animal facilities on a 12-hour light/dark cycle with access ad libitum to food and water.

### 2.3. Intact vs cultured mouse dorsal root ganglia

#### 2.3.1. Price laboratory

Male and female C57BL/6 mice (4 week-old, ~15–20 g; n = 3, for each sex) were anesthetized with isoflurane and killed by decapitation. Male C57BL/6 mice (5 week-old, n = 2) were used

for RNAscope validation. Mice were not perfused before removal of DRG. Lumbar DRG (L1–L6) from one side of the spine were frozen in RNAlater (Invitrogen, Carlsbad, CA) while DRG from the other side from the same mouse were cultured and then scraped at 4 DIV into RNAlater. All L1–L6 DRG were used for RNAscope validation. L1–L6 DRG for culturing were dissected and placed in chilled HBSS (Invitrogen) until processed. Dorsal root ganglia were then digested in 1-mg/mL collagenase A (Roche, Indianapolis, IN) for 25 minutes at 37°C then subsequently digested in 1-mg/mL collagenase D for 20 minutes at 37°C. Dorsal root ganglia were then triturated in 1-mg/mL trypsin inhibitor (Roche), then filtered through a 70- $\mu$ m cell strainer (Corning, Oneonta, NY). Cells were pelleted, and then resuspended in DMEM/F12 with GlutaMAX (Thermo Fisher Scientific, Carlsbad, CA) containing 10% fetal bovine serum (Thermo Fisher Scientific), 1% penicillin and streptomycin, 5-ng/mL mouse 2.5S nerve growth factor (Millipore, Billerica, MA), and 3- $\mu$ g/mL 5-fluorouridine with 7- $\mu$ g/mL uridine. Cells were distributed evenly across 4 wells using a 24-well plate coated with poly-D-lysine (Becton Dickinson, Franklin Lakes, NJ). For RNAscope validation cultures, cells were plated as described on an 8-well chamber slide (Nunc Lab-Tek, Naperville, IL). Dorsal root ganglion neurons were maintained in a 37°C incubator containing 5% CO<sub>2</sub> with a media change every other day. At 4 DIV, cells were scraped into 500- $\mu$ L RNAlater and processed for RNA extraction.

#### 2.3.2. Gereau laboratory

Male and female C57BL/6 mice (n = 3, for each sex) were deeply anesthetized with isoflurane and quickly decapitated. Mice were not perfused before removal of DRG. From one side, L1–6 DRG were extracted, directly placed into 500- $\mu$ L RNAlater, and stored at –80°C. From the other side, L1–6 DRG were extracted and dissociated in freshly made *N*-methyl-D-glucamine (NMDG) solution (Valtcheva et al.). Dorsal root ganglia were digested in 15-U/mL papain (Worthington Biochemical, Lakewood, NJ) for 20 minutes at 37°C, washed, and then further digested in 1.5-mg/mL collagenase type 2 (Sigma, St Louis, MO) for another 20 minutes at 37°C. Dorsal root ganglia were washed and triturated in DRG media (5% fetal bovine serum [Gibco, Carlsbad, CA] and 1% penicillin/streptomycin [Corning] in Neurobasal A medium 1x [Gibco] plus Glutamax [Life Technologies, Carlsbad, CA] and B27 [Gibco]). Final solutions of cells were filtered (40  $\mu$ m, Fisher) and cultured in DRG media on coverslips coated with poly-D-lysine (Sigma) and rat tail collagen (Sigma). Cultures were maintained in an incubator at 37°C containing 5% CO<sub>2</sub>. On 4 DIV (no media changes), cultured coverslips were scraped in 500- $\mu$ L RNAlater and stored at –80°C.

### 2.4. Intact vs cultured human dorsal root ganglia

Studies involving human DRG were performed on deidentified biospecimens and approved by Institutional Review Boards at Washington University in St. Louis and University of Texas at Dallas.

#### 2.4.1. Gereau laboratory

Human DRG extraction and culturing was performed as described previously (Valtcheva et al.), in a similar manner to the mouse culturing protocol. Briefly, in collaboration with Mid-America Transplant Services, L4–L5 DRG were extracted from tissue/organ donors less than 2 hours after aortic cross clamp. Donor information is presented in **Table 1**. Dorsal root ganglia were placed in NMDG solution for transport to the laboratory for fine dissection. From one side, intact L4–5 DRG were directly

**Table 1**  
**Human DRG donor characteristics and donor–sample mapping.**

Donor id	Age	Sex	Race	Cause of death	Sample ids
1	53	F	White	ICH/stroke	hDRG-1F, hDRG-1Fre, hDIV4-1F, and hDIV4-1Fre
2	12	F	White	Anoxia/OD	hDRG-2F, hDIV4-2F
3	26	M	White	Head trauma/MVA	hDRG-3M, hDIV4-3M
4	34	M	White	Anoxia/OD	hDRG-4M, hDIV4-4M
5	18	F	White	Head trauma/MVA	hDRG-5F, hDIV4-5F
6	18	M	White	Head trauma/GSW	hDRG-6M, hDIV4-6M

DIV, days in vitro; DRG, dorsal root ganglion ICH, intra-cerebral hemorrhage; OD, oxygen deprivation; MVA, motor vehicle accident; GSW, gunshot wound.

placed into 500- $\mu$ L RNAlater and stored at  $-80^{\circ}\text{C}$ . From the other side, L4-5 DRG were minced and cultured. Pieces were dissociated enzymatically with papain and collagenase type 2 for 1 hour each and mechanically with trituration. Final solutions were filtered (100  $\mu\text{m}$ , Fisher) and cultured with DRG media. On 4 DIV, cultured coverslips were scraped in 500- $\mu$ L RNAlater and stored at  $-80^{\circ}\text{C}$ .

### 2.5. RNA sequencing

Human and mouse DRG tissue/cultured cells were stored in RNAlater and frozen in  $-80^{\circ}\text{C}$  until use. Samples obtained at the Washington University at St Louis were shipped to UT Dallas on dry ice for uniform library preparation. All RNA isolation and sequencing was performed in the Price laboratory. On the day of use, the frozen tubes were thawed to room temperature. To obtain RNA from tissue samples, the tissue was extracted from RNAlater with ethanol cleaned tweezers and put in 1 mL of QIAzol (QIAGEN, Inc, Valencia, CA) inside 2-mL tissue homogenizing CKMix tubes (Bertin Instruments, Rockville, MD). To obtain RNA from cell cultures, cells were spun down to the bottom of the tube by centrifuge at 5000g for 10 minutes. RNAlater was then removed from the tube, and cells were resuspended with 1 mL of QIAzol and transferred to the homogenizing tube. For both tissues and cell cultures, homogenization was performed for  $3 \times 1$  minute with Minilys personal homogenizer (Bertin Instruments) at  $4^{\circ}\text{C}$ . This time course was used to avoid heating during homogenization. RNA extraction was performed with RNeasy Plus Universal Mini Kit (QIAGEN, Inc) with the manufacturer provided protocol. RNA was eluted with 30  $\mu\text{L}$  of RNase free water. Based on the RNA size profile determined by the Fragment Analyzer (Agilent Technologies, Santa Clara, CA) with the High Sensitivity Next Generation Sequencing fragment analysis kit, we decided to sequence all human samples with total RNA library preparation and all mouse samples with mRNA library preparation. Total RNA was purified and subjected to TruSeq stranded mRNA library preparation for mouse or total RNA Gold library preparation (with ribosomal RNA depletion) for human, according to the manufacturer's instructions (Illumina, San Diego, CA). Quality control was performed for RNA extraction and cDNA library preparation steps with Qubit (Invitrogen) and High Sensitivity Next Generation Sequencing fragment analysis kit on the Fragment Analyzer (Agilent Technologies). After standardizing the amount of cDNA per sample, the libraries were sequenced on an Illumina NextSeq500 sequencing platform with 75-bp single-end reads in multiplexed sequencing experiments, yielding a median of 22.3 million reads per sample. mRNA library preparation and sequencing was prepared at the Genome Center in the University of Texas at Dallas Research Core Facilities.

### 2.6. RNAscope-based imaging

RNAscope in situ hybridization (multiplex version 1)<sup>65</sup> assays were conducted based on Advanced Cell Diagnostics (ACD) protocols.

#### 2.6.1. Intact dorsal root ganglia

Fresh frozen lumbar DRG were rapidly dissected, frozen in cryomolds with O.C.T (Fisher Scientific; Cat# 23-730-571) over dry ice, and sectioned at 20  $\mu\text{m}$  onto charged slides. The sections were fixed in cold ( $4^{\circ}\text{C}$ ) 10% formalin for 15 minutes and then dehydrated in 50% ethanol (5 minutes), 70% ethanol (5 minutes), and 100% ethanol (10 minutes) at room temperature. Slides were briefly air dried, and boundaries were then drawn around each section using the hydrophobic ImmEdge PAP pen (Vector Labs, Burlingame, CA). When hydrophobic boundaries had dried, protease IV reagent was used to incubate the sections for 2 minutes and then washed in 1X phosphate-buffered saline (PBS). Every slide was placed in a prewarmed humidity control tray (ACD) with dampened filter paper and incubated in a mixture of channel 1 (*Cd68*; ACD Cat# 316611), channel 2 (*Calca*; ACD Cat#417961), and channel 3 (*P2rx3*; ACD Cat# 521611) probes for 2 hours at  $40^{\circ}\text{C}$ . This was performed one slide at a time to avoid liquid evaporation and section drying. After probe incubation, the slides were washed 2 times in 1X RNAscope wash buffer, submersed in AMP-1 reagent, and returned to the oven for 30 minutes. Washes and amplification were repeated using AMP-2, AMP-3, and AMP-4B reagents with 15-, 30-, and 15-minute incubation period, respectively. Slides were then washed 2 times in 0.1 M phosphate buffer (PB, pH7.4) and then submerged in blocking reagent (10% Normal Goat serum and 0.3% Triton-X 100 in 0.1 M PB) for 1 hour at room temperature. Slides were incubated in primary antibody (mouse-anti-Neurofilament 200; clone N52; Sigma) at 1:500 in blocking buffer overnight at  $4^{\circ}\text{C}$ . The next day, slides were washed 2 times in 0.1 M PB and then incubated in secondary antibody (goat-anti-mouse H&L 405; 1:2000) for 1 hour at room temperature. Sections were washed 2 times in 0.1 M PB, air dried, and cover-slipped with Prolong Gold Antifade (Fisher Scientific; Cat# P36930) mounting medium.

#### 2.6.2. Cultured dorsal root ganglia

At 4 DIV (no media change), media were aspirated from each well and the chambers disassembled from the slide. The slide was washed once in 1X PBS and fixed for 30 minutes at room temperature in 10% formalin. Slides were then washed twice in 1X PBS after which RNAscope in situ hybridization was performed as

described above with the noted changes. Protease incubation was 10 minutes at room temperature with protease III reagent (1:30 in 1X PBS). Probe incubation used a channel 1 (Cd68) probe. Permeabilizing reagent (0.02% Triton-X 100) was added to blocking buffer (10% normal goat serum in 0.1 M PB) only for the one-hour blocking step. Slides were incubated in primary (rabbit-anti-peripherin; 1:1000; Sigma) and secondary (goat-anti-rabbit H&L 488; 1:2000) antibodies as described. Slides were washed once in 0.1 M PB and incubated in 4',6-diamidino-2-phenylindole (DAPI) (1:5000) for 5 minutes at room temperature before washing, mounting, and imaging as described.

### 2.6.3. Imaging

All images were taken on an Olympus FV3000 confocal microscope using the 20× and 40× objectives. Images were pseudocolored to show 4 distinct color frequencies and overlaid, using the CellSens software (Olympus).

## 2.7. Computational analysis

### 2.7.1. Mapping and transcripts per million quantification

RNA-seq read files (fastq files) were checked for quality by FastQC (Babraham Bioinformatics, <https://www.bioinformatics.babraham.ac.uk/projects/fastqc/>), and read trimming was performed based on the Phred score and per-base sequence content (base pairs 13 through 72 were retained). Trimmed Reads were then mapped against the reference genome and transcriptome (Gencode vM16 and GRCm38.p5 for mouse, Gencode v27 and GRCh38.p10 for human<sup>22</sup>) using STAR v2.2.1.<sup>18</sup> Relative abundances in transcripts per million (TPM) for every gene of every sample was quantified by stringtie v1.3.5.<sup>48</sup> Downstream analyses were restricted to protein coding genes to make human (total RNA) and mouse (polyA+ RNA) libraries comparable; hence, TPMs of only genes annotated as coding genes in the Gencode database were renormalized to sum to a million. Sequencing and mapping statistics reported by STAR are presented in **Table 2**.

### 2.7.2. Hierarchical clustering

RNA-seq samples for each species were analyzed for similarity by performing hierarchical clustering. The distance metric used for clustering was  $(1 - \text{correlation coefficient})$  based on the Pearson correlation coefficient,<sup>46</sup> and average linkage was used to generate the dendrogram from the distance matrix. The hierarchical clustering was then used to determine whether there were any transcriptome-wide differences in the RNA profiles based on sex or based on technical factors that were changing across laboratories (for the mouse samples).

### 2.7.3. Outlier analysis

In human cultured DRG samples, we detected an outlier (sample id hDIV4-1F, **Fig. 1A**). To rule out incorrect library construction, we sequenced this sample again using another independently prepared library. However, the new library was still an outlier on sequencing but very similar to the original library (suggesting low technical variability in our library preparation and sequencing steps). In contrast to the other human DRG cultures, this sample had negligible expression levels for many neuronal markers such as *CALCA*, *TRPV1*, and *SCN10A*

(Supplementary file 1, sheet 1, available at <http://links.lww.com/PAIN/A983>), suggesting that few neurons survived the culturing process for this sample. Consistent with this, experimental notes regarding cultures from hDIV4-1F indicated very sparse apparent neurons in the cultures (not shown). Thus, this sample and its paired intact DRG sample (sample id hDRG-1F) were excluded from further analysis. A mouse outlier sample (sample id mDIV4-4Fg, **Fig. 1B**) was similarly analyzed, but expression of neuronal marker genes was considered sufficient for retention in the analysis.

### 2.7.4. Identification of consistently detectable genes

Previous studies on whole DRG tissue have found functional responses for G-protein-coupled receptors (GPCRs) with < 0.4 TPMs (eg, *GRM2* functionally studied and abundance quantified in the papers<sup>16,51</sup>). This suggests that the approach of picking an expression threshold (in TPMs) to classify a gene either as “on” or “off” is likely to miss functionally relevant gene products based on traditional thresholds (~1 TPM, as in North et al.<sup>43</sup>). Instead, we classified consistently detectable genes based on reads being detected in the exonic region in 80% or more of the samples in a particular condition (ie, in at least 4 of 5 human replicates, or in at least 10 of 12 mouse replicates). Assuming iid probabilities for detecting a read emanating from a particular gene in an RNA-seq experiment, this criterion causes the sensitivity of our approach to be suitable for our purpose, calling consistently detectable genes to be those that have  $\geq 1$  read in 7 million coding gene reads in an RNA-seq library, as:

$$1 - \left(1 - \frac{1}{7 \times 10^6}\right)^{11 \times 10^6} = 0.792 \approx 0.8$$

(all of our RNA-seq datasets have > 11 million reads mapping to coding gene exons)

### 2.7.5. Differential expression metrics

Owing to small sample sizes in humans, stringent statistical hypothesis testing using the Student *t* test<sup>56</sup> with Benjamini-Hochberg multitesting correction<sup>4</sup> yields few statistically significant differences.

We therefore decided to use strictly standardized mean difference (SSMD) to discover genes with systematically altered expression levels between experimental conditions. For each human and mouse coding gene, we report fold change and the SSMD across conditions. Standardized mean difference is the difference of means controlled by the variance of the sample measurements. We used SSMD as a secondary effect size since it is well suited for small sample sizes as in our human samples,<sup>43,77</sup> while simultaneously taking into account the dispersion of the data points. For determining SSMD thresholds that identify genes that are systematically changing between conditions, we use the notion of the related Bhattacharyya coefficient,<sup>7</sup> which is used to calculate the amount of overlap in the area under the curve of the 2 sample distributions to control for false positives in differential expression analysis. For homoskedastic Gaussian distributions, we find that based on the Bhattacharyya coefficient, the less stringent constraint  $\text{ISSMDI} > 2.0$  corresponds to a 36.8% overlap in the area under the curve of the 2 sample distributions being tested, while the more stringent

**Table 2**  
**Statistics for RNA-seq experiments.**

Sample id	No. of reads sequenced	No. of reads mapped	No. of reads mapped uniquely	No. of coding genes detected
mDRG-1Mg	22,212,434	21,048,941	16,559,517	15,749
mDRG-2Mg	19,189,967	18,300,700	14,957,918	15,626
mDRG-3Mg	22,487,076	21,509,723	17,478,260	15,731
mDRG-4Fg	22,509,372	21,402,718	17,608,765	15,719
mDRG-5Fg	19,655,816	18,756,552	15,205,161	15,619
mDRG-6Fg	23,274,760	22,290,521	18,174,167	15,828
mDRG-1Mp	14,877,799	14,315,363	11,760,256	15,536
mDRG-2Mp	15,635,533	15,082,808	12,348,811	15,593
mDRG-3Mp	16,808,435	16,186,083	13,173,528	15,797
mDRG-4Fp	15,577,724	14,993,698	12,189,645	15,631
mDRG-5Fp	15,316,097	14,756,450	11,993,815	15,638
mDRG-6Fp	16,108,903	15,531,301	12,558,411	15,707
mDIV4-1Mg	19,520,498	18,593,009	15,426,436	15,193
mDIV4-2Mg	23,861,527	22,827,565	18,645,619	15,402
mDIV4-3Mg	22,706,726	21,755,398	17,668,475	15,520
mDIV4-4Fg	14,769,253	13,761,459	10,464,363	15,078
mDIV4-5Fg	21,735,780	20,745,007	16,544,691	15,362
mDIV4-6Fg	21,313,704	20,495,656	16,698,375	15,463
mDIV4-1Mp	15,572,289	14,959,958	11,966,895	14,879
mDIV4-2Mp	16,189,281	15,581,390	12,564,211	15,105
mDIV4-3Mp	17,299,306	16,653,412	13,433,467	15,025
mDIV4-4Fp	15,873,155	15,285,290	12,296,395	14,778
mDIV4-5Fp	14,300,332	13,735,983	11,025,628	14,767
mDIV4-6Fp	16,582,457	15,955,531	12,832,261	14,991
hDRG-1F	37,683,580	35,740,910	12,227,687	15,590
hDRG-1Fre	60,648,611	58,374,576	19,659,672	16,016
hDRG-2F	45,504,043	43,479,464	16,157,986	15,881
hDRG-3M	43,890,090	41,819,026	14,804,561	15,656
hDRG-4M	83,956,740	79,390,702	27,625,219	16,507
hDRG-5F	44,290,887	42,269,829	15,481,526	15,594
hDRG-6M	39,464,882	36,862,011	12,529,277	15,684
hDIV4-1F	29,815,327	28,497,933	9,368,106	14,420
hDIV4-1Fre	42,975,599	40,614,264	15,459,290	15,230
hDIV4-2F	35,923,946	34,767,067	19,764,235	14,886
hDIV4-3M	37,956,210	36,724,983	19,909,457	14,979
hDIV4-4M	49,113,664	47,509,436	26,123,855	15,253
hDIV4-5F	27,378,169	26,484,024	12,695,780	14,388
hDIV4-6M	36,524,530	35,316,646	19,947,805	14,829

DIV, days in vitro; DRG, dorsal root ganglia.

ISSMDI > 3.0 corresponds to a 10.5% overlap. The less stringent criterion was used to select differentially expressed genes in gene sets of pharmacological interest, since genes with a moderate amount (<36.8%) of overlap in TPM distributions between intact and cultured DRG should likely not be targeted for pharmacological purposes. The more stringent constraint corresponding to little or no overlap in sample distributions (<10.5%) was used to identify differentially expressed genes at the genome-wide level.

Since our data are paired, we report several variations of the standard fold change metric. We calculated the ratio of means across conditions to not only compare cohort-level statistics but also calculate the mean of ratios of paired samples to better control for individual to individual variations in the transcriptome. However, the mean of ratios is more susceptible to outlier values, so we further modified it to calculate the median of ratios. All fold changes are reported as  $\log_2$  fold changes, for symmetric scaling of fold changes in both directions. Since naive filtering or ranking by log-fold change can produce incorrect results,<sup>49</sup> we constrain differentially expressed genes by SSMD threshold. However, we

do additionally constrain that the fold change (ratio of means or median of ratios) be >1.5, since dosage-based functional effects are unlikely to be manifested as a result of lower fold changes.

To avoid issues in calculations of these metrics for genes with no detectable reads in one or both conditions, a smoothing factor of 0.01 was added to both the numerator and denominator when calculating fold changes and to the denominator when calculating the SSMD. We also provide uncorrected *P* values for paired, 2-sample, 2-tailed *t* tests conducted for individual genes.

These cohort and intercohort statistics, along with individual sample TPMs, and cohort means, are provided in Supplementary file 1, sheets 1 and 2, available at <http://links.lww.com/PAIN/A983>.

### 2.7.6. Estimation of density functions

To estimate the density functions of fold change (ratio of means) and SSMD for human and mouse pharmacologically relevant genes, we used the inbuilt *ksdensity* function in Matlab, using normal kernel smoothing.

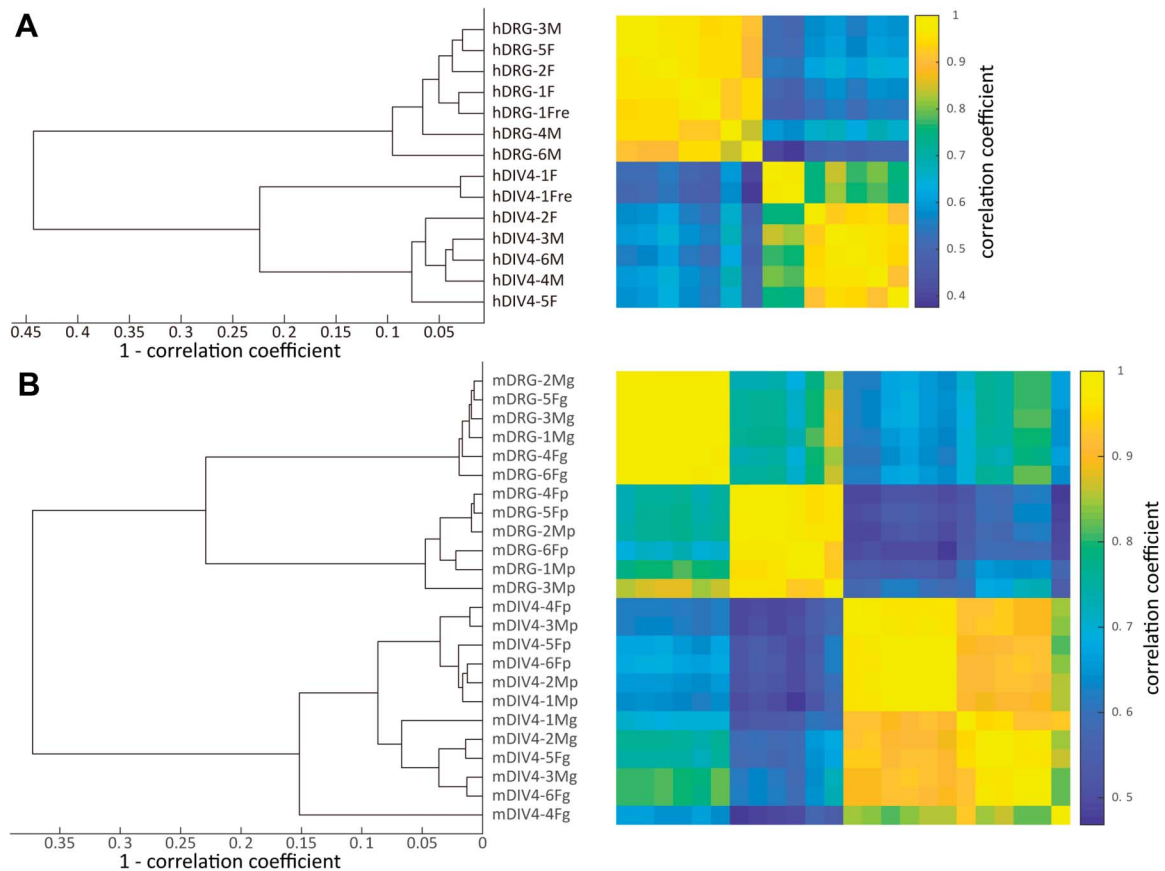


**Figure 1.** Hierarchical clustering of all human (A) and mouse (B) samples based on TPM-based whole genome gene abundances. (A) Cultured and intact human DRG tissue samples are separated into 2 clusters. The outlier sample hDIV-1F and its paired dissected sample (hDRG-1F) were excluded from further analysis. (B) Cultured and intact mouse DRG samples also segregate into separate clusters. Subclusters in the cultured DRG and dissected DRG clusters correspond to sample generated in Gereau and Price laboratories. The outlier sample mDIV4-4Fg shows moderate expression of neuronal genes, and clusters with other Gereau laboratory cultured samples when unrooted clustering is performed for cultured mouse DRG samples. (Sample id nomenclature—Prefix: h, human; m, mouse; Infix: DRG, intact DRG samples; DIV4, 4 days in vitro (4 DIV) DRG cultures; Suffix: M, male; F, female; p, Price laboratory; g, Gereau laboratory; re, repeated library preparation and sequencing. DRG, dorsal root ganglia.

### 2.7.7. Human–mouse gene orthology mapping and gene expression change comparisons across species

Orthologous genes with a one-to-one mapping between human and mouse genomes were identified using the Ensembl database.<sup>25</sup> Genes from the relevant gene families (GPCRs, ion channels, kinases) were removed from analysis if one-to-one orthology was not identified between human and mouse genes. In addition, because of the complicated nature of the orthology map in the olfactory receptor and TAS2R families in mice and human,<sup>15,72</sup> these genes families were also excluded from analysis. For all remaining genes in these families that were consistently detected in human or mouse samples, a trend score was calculated by multiplying the SSMD and log median of paired fold change values. The correlation of the human and mouse trend scores were calculated using Pearson's *R*.<sup>46</sup> Genes not consistently detected in samples of either species were left out of the analysis to avoid inflating the correlation based on the trend scores.

### 2.7.8. Marker gene list compilation

Gene lists used in the paper (ion channel, GPCR, kinase) were acquired from online databases including the Gene Ontology

(AMIGO), HUGO Gene Nomenclature Committee and the Human Kinome database.<sup>20,35,58</sup>

Marker gene lists for constituent cell types in the DRG were sourced from the literature and validated in a recently published mouse nervous system single cell RNA-seq database published by Zeisel et al.<sup>75</sup> We found that many of the traditional protein-based fluorescence markers for these cell types were not ideal for our analyses. Of the 49 marker genes we sourced from the literature, we looked for enrichment in the relevant cell subpopulations in the Zeisel et al. database. Since PNS macrophages and PNS vascular cells were not profiled in the database, the maximum expression levels in subpopulations of central nervous system (CNS) immune cells/microglia and CNS vascular cells profiled in the database were used as surrogates. Genes that had expression levels in the Zeisel et al. database that were 2-fold (or greater) higher in at least one of the subpopulations of the relevant cell type compared with the other constituent DRG cell types (or their surrogates) were considered to be enriched in the corresponding cell types. Of the 49 marker genes we sourced from the literature, only 34 were found to be enriched in the relevant cell types and were subject to statistical hypothesis testing using paired *t*-tests. Benjamini–Hochberg correction for false discovery rate control was performed on

these genes since this gene set was determined pre hoc. A complete list of the 49 genes and their expression levels in cultured and intact DRG, along with statistical hypothesis testing on the 34 validated marker genes, is provided in **Table 3**.

Based on our analysis in the Zeisel et al. database, the literature-based markers *Gap43*, *Ncam1*, and *Ncam2* for non-myelinating Schwann cells were also found to be expressed in satellite glial cells (SGCs) and/or neurons. Similarly, SGC markers

**Table 3**  
Differential expression analysis in human and mouse DRG for constituent cell type marker genes.

HUMAN DATASETS							MOUSE DATASETS						
Ensembl gene id	Ensembl gene name	Cultured DRG mean	Acutely dissected DRG mean	SSMD (smoothed)	Uncorrected paired, 2-tailed t-test p-value	Is B-H FDR correction at $\alpha = 0.05$ statistically significant?	Ensembl gene id	Ensembl gene name	Cultured DRG mean	Acutely dissected DRG mean	SSMD (smoothed)	Uncorrected paired, 2-tailed t-test p-value	Is B-H FDR correction at $\alpha = 0.05$ statistically significant?
<b>Literature-based neuronal subpopulation markers, with mouse Zeisel et al scRNA-seq expression enriched in DRG neurons</b>													
ENSG00000167281.18	RBFOX3	0.3	24.9	-3.0	0.003	TRUE	ENSMUSG00000025576.17	Rbfox3	33.0	253.7	-4.6	0.000	TRUE
ENSG00000110680.12	CALCA	220.5	675.2	-3.7	0.001	TRUE	ENSMUSG00000030669.13	Calca	857.3	3572.5	-4.6	0.000	TRUE
ENSG00000175868.13	CALCB	52.8	245.7	-5.5	0.000	TRUE	ENSMUSG00000030666.11	Calcb	42.0	308.5	-4.2	0.000	TRUE
ENSG00000142185.16	TRPM2	10.0	43.1	-3.1	0.005	TRUE	ENSMUSG00000009292.18	Trpm2	0.9	23.2	-3.5	0.000	TRUE
ENSG00000196689.11	TRPV1	13.0	128.1	-5.6	0.000	TRUE	ENSMUSG00000005952.15	Trpv1	29.9	115.2	-3.5	0.000	TRUE
ENSG00000154864.11	PIEZO2	15.8	148.6	-7.0	0.000	TRUE	ENSMUSG00000041482.16	Piezo2	41.8	111.6	-2.1	0.000	TRUE
ENSG00000100285.9	NEFH	57.4	1153.1	-8.4	0.000	TRUE	ENSMUSG00000020396.8	Nefh	109.8	1379.3	-7.4	0.000	TRUE
ENSG00000277586.2	NEFL	81.5	1127.3	-6.6	0.000	TRUE	ENSMUSG00000022055.7	Nefl	612.6	3928.3	-5.5	0.000	TRUE
ENSG00000104722.13	NEFM	14.7	501.1	-9.3	0.000	TRUE	ENSMUSG00000022054.11	Nefm	309.0	2524.0	-4.8	0.000	TRUE
ENSG00000135406.13	PRPH	333.6	2225.8	-2.1	0.018	TRUE	ENSMUSG00000023484.13	Prph	919.2	3083.2	-3.5	0.000	TRUE
ENSG00000164220.6	F2RL2	1.4	11.4	-6.5	0.000	TRUE	ENSMUSG00000021675.4	F2rl2	14.2	86.0	-4.1	0.000	TRUE
<b>Literature-based Schwann cell subpopulation markers, with mouse Zeisel et al scRNA-seq expression enriched in Schwann cells</b>													
ENSG00000158887.15	MPZ	190.3	1984.1	-5.6	0.000	TRUE	ENSMUSG00000056569.10	Mpz	211.5	13564.9	-1.2	0.002	TRUE
ENSG00000197971.14	MBP	63.5	592.0	-2.9	0.004	TRUE	ENSMUSG00000041607.16	Mbp	200.8	1186.5	-1.1	0.004	TRUE
<b>Literature-based neural tissue vascular cell subpopulation markers, with mouse Zeisel et al scRNA-seq expression enriched in CNS vascular cells</b>													
ENSG00000197467.13	COL13A1	15.7	1.1	2.3	0.006	TRUE	ENSMUSG00000058806.14	Col13a1	0.5	1.0	-0.4	0.209	FALSE
ENSG00000204291.10	COL15A1	489.9	87.4	2.6	0.002	TRUE	ENSMUSG00000028339.17	Col15a1	206.7	40.3	1.4	0.000	TRUE
ENSG00000168542.14	COL3A1	5873.5	273.4	2.6	0.004	TRUE	ENSMUSG00000026043.18	Col3a1	682.9	109.0	2.3	0.000	TRUE
ENSG00000187498.14	COL4A1	901.3	344.0	5.2	0.000	TRUE	ENSMUSG00000031502.11	Col4a1	824.2	115.7	4.0	0.000	TRUE
ENSG00000134871.17	COL4A2	661.4	413.8	2.9	0.001	TRUE	ENSMUSG00000031503.13	Col4a2	648.9	89.2	3.4	0.000	TRUE
ENSG00000188153.12	COL4A5	3.6	32.6	-3.5	0.002	TRUE	ENSMUSG00000031274.16	Col4a5	4.8	1.3	1.5	0.000	TRUE
ENSG00000204262.11	COL5A2	933.5	95.6	3.8	0.001	TRUE	ENSMUSG00000026042.16	Col5a2	1311.2	26.5	2.5	0.000	TRUE
ENSG00000142156.14	COL6A1	760.6	351.8	2.4	0.003	TRUE	ENSMUSG00000001119.7	Col6a1	140.6	35.9	1.4	0.000	TRUE
ENSG00000142173.14	COL6A2	1660.9	446.3	3.5	0.000	TRUE	ENSMUSG00000020241.13	Col6a2	49.8	41.2	0.5	0.014	TRUE
ENSG00000163359.15	COL6A3	676.8	65.5	5.5	0.000	TRUE	ENSMUSG00000048126.16	Col6a3	119.6	10.4	2.0	0.000	TRUE
ENSG00000115414.18	FN1	5452.9	476.4	3.3	0.002	TRUE	ENSMUSG00000026193.15	Fn1	1160.4	36.9	2.1	0.000	TRUE
<b>Literature-based neural tissue immune cell subpopulation markers, with mouse Zeisel et al scRNA-seq expression enriched in CNS immune cells</b>													
ENSG00000129226.13	CD68	91.6	41.6	0.9	0.111	FALSE	ENSMUSG00000018774.13	Cd68	63.4	6.6	3.2	0.000	TRUE
<b>Literature-based Satellite Glial Cell subpopulation markers, with mouse Zeisel et al scRNA-seq expression enriched in proliferating SGCs</b>													
ENSG00000117399.13	CDC20	77.4	6.9	2.5	0.005	TRUE	ENSMUSG00000006398.15	Cdc20	130.0	3.3	8.7	0.000	TRUE
ENSG00000168078.9	PBK	23.0	0.3	1.5	0.027	TRUE	ENSMUSG00000022033.9	Pbk	98.0	0.7	5.3	0.000	TRUE
ENSG00000175063.16	UBE2C	76.9	1.3	3.2	0.001	TRUE	ENSMUSG00000001403.13	Ube2c	222.4	1.9	4.8	0.000	TRUE
ENSG00000089685.14	BIRC5	23.3	2.3	1.8	0.015	TRUE	ENSMUSG00000017716.15	Birc5	178.7	7.8	7.4	0.000	TRUE
<b>Literature-based Satellite Glial Cell subpopulation markers, with mouse Zeisel et al scRNA-seq expression enriched in proliferating SGCs, also expressed in all SGCs</b>													
ENSG00000219435.5	CATSPERZ	0.1	3.3	-2.2	0.010	TRUE	ENSMUSG00000050623.4	Catsperz	2.8	24.4	-4.7	0.000	TRUE
<b>Literature-based Satellite Glial Cell subpopulation markers, with mouse Zeisel et al scRNA-seq expression enriched in all SGCs</b>													
ENSG00000163520.13	FBLN2	138.4	141.1	0.0	0.919	FALSE	ENSMUSG00000064080.12	Fbln2	1674.7	143.1	4.2	0.000	TRUE
ENSG00000107165.12	TYRP1	0.1	2.8	-1.9	0.015	TRUE	ENSMUSG00000005994.14	Tyrp1	3.1	11.2	-2.0	0.000	TRUE
ENSG00000146250.6	PRSS35	2.0	0.3	2.1	0.013	TRUE	ENSMUSG00000033491.13	Prss35	41.0	28.5	0.9	0.018	TRUE
<b>Literature-based Satellite Glial Cell subpopulation markers, with mouse Zeisel et al scRNA-seq expression enriched in all SGCs, also expressed in Schwann cells</b>													
ENSG00000140092.14	FBLN5	145.9	293.5	-2.1	0.002	TRUE	ENSMUSG00000021186.9	Fbln5	91.3	51.5	0.6	0.029	TRUE
<b>Literature-based neuronal subpopulation markers, with undetectable mouse DRG expression</b>													
ENSG00000072315.3	TRPC5	0.7	3.4	Not shown	Not shown	Not shown	ENSMUSG000000041710.4	Trpc5	0.0	0.0	Not shown	Not shown	Not shown
<b>Literature-based neuronal subpopulation markers, with mouse Zeisel et al scRNA-seq expression enriched in other cell types alongside DRG neurons</b>													
ENSG00000124813.20	RUNX2	133.3	34.1	Not shown	Not shown	Not shown	ENSMUSG000000039153.16	Runx2	20.7	2.3	Not shown	Not shown	Not shown
<b>Literature-based Schwann cell subpopulation markers, with mouse Zeisel et al scRNA-seq expression enriched in other cell types alongside Schwann cells</b>													
ENSG00000172020.12	GAP43	105.8	60.8	Not shown	Not shown	Not shown	ENSMUSG000000047261.9	Gap43	483.4	385.0	Not shown	Not shown	Not shown
ENSG00000149294.16	NCAM1	74.2	478.5	Not shown	Not shown	Not shown	ENSMUSG000000039542.16	Ncam1	162.6	65.0	Not shown	Not shown	Not shown
ENSG00000154654.14	NCAM2	3.8	33.1	Not shown	Not shown	Not shown	ENSMUSG00000002762.17	Ncam2	1.5	2.0	Not shown	Not shown	Not shown
<b>Literature-based neural tissue vascular cell subpopulation markers, with mouse Zeisel et al scRNA-seq expression enriched in other cell types alongside CNS vascular cells</b>													
ENSG00000196739.14	COL27A1	11.3	121.6	Not shown	Not shown	Not shown	ENSMUSG000000045672.15	Col27a1	23.1	12.5	Not shown	Not shown	Not shown
ENSG00000150093.18	ITGB1	1271.5	303.9	Not shown	Not shown	Not shown	ENSMUSG000000025809.15	Itgb1	1346.0	202.6	Not shown	Not shown	Not shown
<b>Literature-based neural tissue immune cell subpopulation markers, with mouse Zeisel et al scRNA-seq expression enriched in other cell types alongside CNS immune cells</b>													
ENSG00000130203.9	APOE	1015.5	1152.0	Not shown	Not shown	Not shown	ENSMUSG00000002985.16	Apoe	517.6	3483.4	Not shown	Not shown	Not shown
ENSG00000164434.11	FABP7	457.6	596.0	Not shown	Not shown	Not shown	ENSMUSG000000019874.11	Fabp7	603.3	590.2	Not shown	Not shown	Not shown
ENSG00000155368.16	DBI	529.3	347.6	Not shown	Not shown	Not shown	ENSMUSG000000026385.16	Dbi	1714.6	1027.7	Not shown	Not shown	Not shown
ENSG00000121594.11	CD80	3.5	2.7	Not shown	Not shown	Not shown	ENSMUSG000000075122.4	Cd80	25.4	0.2	Not shown	Not shown	Not shown
ENSG00000184557.4	SOC3	5.0	2.4	Not shown	Not shown	Not shown	ENSMUSG000000053113.3	Socs3	79.9	11.2	Not shown	Not shown	Not shown
<b>Literature-based Satellite Glial Cell subpopulation markers, with mouse Zeisel et al scRNA-seq expression enriched in other cell types alongside SGCs</b>													
ENSG00000139549.2	DHH	3.7	13.1	Not shown	Not shown	Not shown	ENSMUSG00000023000.4	Dhh	102.6	85.5	Not shown	Not shown	Not shown
ENSG00000170312.15	CDK1	34.9	2.9	Not shown	Not shown	Not shown	ENSMUSG000000019942.13	Cdk1	153.4	2.3	Not shown	Not shown	Not shown
No human ortholog for Ceacam10													
							ENSMUSG000000054169.7	Ceacam10	0.3	17.9	Not shown	Not shown	Not shown

Cultured DRG statistics are shown in yellow, while acutely dissected DRG statistics are shown in blue. SSMDs are shown on a two-color scale with positive SSMDs (increase in cultured DRGs) shown in green, and negative SSMDs (decrease in cultured DRGs) shown in red. CNS, central nervous system; DRG, dorsal root ganglia; SGC, satellite glial cell; SSMD, standardized mean difference.

*Dhh*, *Fbln5*, and *Ceacam10* are expressed in both Schwann cells and SGCs. *Fbnl2*, *Tyrp1*, and *Prss35* were found to be comparably enriched in proliferating and nonproliferating SGCs. Microglial/macrophage markers *Apoe*, *Fabp7*, and *Dbi* were also found to be expressed in SGCs and not used as markers. Finally, *Trpc5* was found to be absent in mouse sensory neurons.

### 2.7.9. Code

Coding was performed in Matlab, and data visualization was performed in Matlab and GraphPad Prism V8. Normalized counts and analysis are presented in a companion website: <https://bbs.utdallas.edu/painneurosciencelab/sensoryomics/culturetxome/>.

## 3. Results

### 3.1. Hierarchical clustering of human and mouse samples reveal whole transcriptome differences between cultured and intact DRG

We used hierarchical clustering to assess differences between RNA-seq samples analyzed in this study. As shown in **Figure 1**, the top-level split of the hierarchical clustering for both human and mouse samples was between cultured and intact DRG tissue, showing consistent whole transcriptome changes between the two. We identified broad changes in the transcriptome between intact and cultured DRG, with 2440 human and 2941 mouse genes having a fold change (ratio of means and median of ratios) > 1.5, and ISSMDI > 3.0 between compared conditions (Supplementary file 1, sheets 1 and 2, available at <http://links.lww.com/PAIN/A983>). The smaller number of changed genes that we detect in human can be attributed to a smaller number of detected genes that increase in abundance in culture in humans compared with mouse. Of the differentially expressed genes, only 443 (18%) of the human genes and 1156 (39%) of the mouse genes have increased abundances in cultured conditions, which suggests that a majority of the differentially expressed genes gain in relative abundance in intact DRG compared with culture. Controlled laboratory conditions and a similar genome (belonging to the same mouse strain) potentially causes lower within-group variation at the level of individual genes in the mouse samples with respect to the human samples. The smaller number of human genes detected to be increasing in culture can likely be attributed to higher within-group variation in human samples, since genes that show significantly increased expression in cultured conditions have more moderate changes (median across ratio of means in genes satisfying differential expression criterion—human: 2.8 fold, mouse: 3.5 fold) in expression compared with genes that show significantly increased expression in intact DRG (median in human: 5.4 fold, mouse: 5.1 fold). They are therefore less likely to be detected in a lower signal to noise ratio scenario.

### 3.2. No distinct differences at the whole transcriptome level across sexes

In both human and mouse samples, we did not find clear sex differences at the whole transcriptome level, although individual sex markers such as *UTY* differ between the sexes (Supplementary file 1, sheets 1 and 2, available at <http://links.lww.com/PAIN/A983>), consistent with previous findings.<sup>34</sup> Thus, male and female samples were grouped together for further analyses.

### 3.3. Small set of differences between cultured mouse dorsal root ganglion transcriptomes across different laboratories

Experiments were performed in 2 laboratories (Gereau laboratory—sample ids with a “g” suffix; and Price laboratory—sample ids with a “p” suffix, **Fig. 1B**) independently for mouse data sets. Although both laboratories used the same strain of mouse, both intact and cultured DRG had a small but distinct transcriptome difference between the 2 laboratories, leading us to analyze the magnitude and nature of the laboratory-specific differences.

Changes in intact DRG RNA profiles across laboratories are likely caused by environmental differences between animal facilities. In addition, although changes in gene expression levels are well known to be different across inbred mouse strains,<sup>60</sup> recent research suggests that even for inbred mouse strains separated for over hundreds of generations, mutation profiles diverge and can cause different outcomes in molecular assays and have been shown to cause changes in immune function-related genes.<sup>12</sup>

Changes in cultured DRG across laboratories can additionally be explained by differences in culturing protocol. Among the genes that have a greater than 2-fold change in expression is *Ngfr* (mean TPM in Price laboratory: 973, in Gereau laboratory: 438), potentially due to the use of nerve growth factor in the culturing process in the Price laboratory. Several genes that were detected in one or both laboratories’ cultures had laboratory-specific expression changes with ISSMDI > 2 and are noted in **Figure 2**. Surprisingly, we saw that interlaboratory transcriptome differences in cultured mouse DRG were smaller in cultured samples with respect to intact DRG (**Fig. 1B**) despite differences in culturing protocols (eg, without nerve growth factor in the Gereau laboratory, and with nerve growth factor in the Price laboratory). This is likely due to the fact that neurons have the most plastic molecular profiles and putatively decline in proportion in cultured DRG.

The small amount of changes in DRG culture between the 2 laboratories can be summarized as follows. A large amount of overlap was found in consistently detected genes for GPCRs (consistently detected in Price laboratory culture: 191, in Gereau laboratory culture: 214, overlap in both laboratories’ cultures: 183; **Fig. 2A**), RKs (consistently detected in Price laboratory culture: 59, consistently detected in Gereau laboratory culture: 66, overlap in both laboratories’ cultures: 57; **Fig. 2B**), and ion channels (consistently detected in Price laboratory culture: 204, in Gereau laboratory culture: 217, overlap in both laboratories’ cultures: 200; **Fig. 2C and D** for summary of numbers).

We find that most genes highlighted in **Figure 2** have low expression levels (high concentration of genes in the region corresponding to mean TPM < 1.0 for one or more laboratories in scatter plots of **Fig. 2**), or low log fold changes across laboratories (high concentration of genes in the proximal region of the line  $x = y$  in scatter plots of **Fig. 2**), or both. This drives the high correlation in RNA profiles between cultured DRG from both laboratories. Most importantly, for a large majority of the genes that are differentially expressed in DRG cultures between the laboratories, the trend of changes between intact and cultured DRG transcriptome was identical, suggesting that though the degree of change is different for these genes between laboratories, the direction of change is consistent. However, we did identify a small set of pharmacologically relevant genes that had moderate or high gene expression (mean TPM > 1.0) in cultured conditions for at least one laboratory, and a 2-fold or greater change in mean TPM between cultures from the 2 laboratories, but trended in opposite directions between intact and cultured DRG

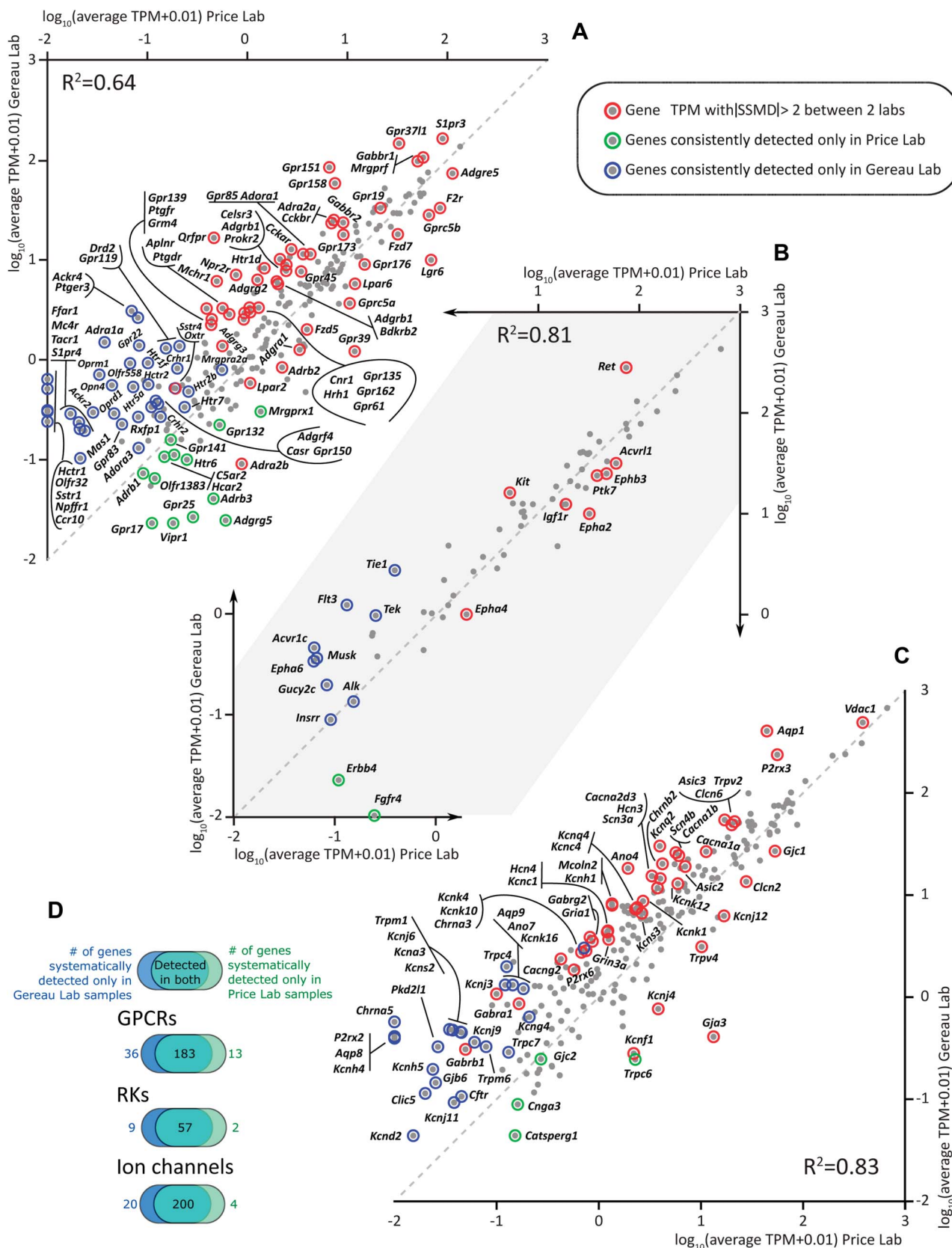


**Figure 2.** Scatter plot and Venn diagrams showing a small amount of differential expression of GPCR genes (A), RK genes (B), and ion channel genes (C) in culture between the Price and Gereau laboratories. The number of genes consistently detected in RNA-sequencing assays for each laboratory is shown in Venn diagrams separated by gene families in (D). Expression levels of genes in all 3 families showed consistent correlation between the 2 laboratories: GPCR genes: Pearson's  $R^2$ : 0.64,  $P < 0.01$ , RK genes: Pearson's  $R^2$ : 0.81,  $P < 0.01$ , ion channel genes: Pearson's  $R^2$ : 0.83,  $P < 0.01$ . Genes such as *Alk* and *Insrr* are plotted on the diagonal, but marked as consistently detected only in Gereau laboratory samples. This is because they have comparable mean TPMs in samples from both laboratories, but are only consistently detected (in 5 or more samples of 6) in the Gereau laboratory. GPCR, G-protein-coupled receptor; TPM, transcripts per million.

transcriptomes. These genes, which consist of 12 GPCRs (*Adgrd1/g3/12/14*, *Adra2a*, *Aplnr*, *Bdkrb2*, *Gpr85/158*, *Gpr3711*, *Mchr1*, and *Prokr2*), 1 RK (*Kdr*), and 10 ion channels (*Aqp1*, *Cacna2d1*, *Gjb2*, *Grid1/2*, *Kcna1/q2*, *Lrrc8b/8d*, and *P2rx3*) show that expression levels for a small set of potential pharmacological targets are influenced by the culturing protocol.

Overall, despite differences in culturing protocol, we find a consistent molecular phenotype in cultured mouse DRG (**Fig. 1B**) in both laboratories that is further explored in the following sections.

### 3.4. Increases in proliferating satellite glial cell and fibroblast markers compensated for by decrease in neuronal and Schwann cell markers in human and mouse cultures

Owing to the magnitude of changes, we tested whether the proportion of mRNA sourced from the different constituent cell types of the DRG were different between intact and cultured samples. We profiled the expression levels of neuron, fibroblast-like cell, Schwann cell, SGC, and macrophage marker genes (chosen based on mouse single cell profiles<sup>75</sup>) in both human and mouse cultured and intact DRG. We found that neuronal markers were broadly downregulated in all cultured samples from mice and humans. Expression levels of neuronal markers in culture were decreased by a median SSMD of 5.55 and 4.20 in human and mouse data sets, respectively (**Table 3**). Conversely, markers for fibroblast-like cells (often of vascular origin) were increased by a median SSMD of 2.90 (human) and 2.03 (mouse) (**Table 3**) in culture compared with intact samples. We found that myelinating Schwann cell markers (*MPZ* and *MBP*) in culture were decreased by a median SSMD of 4.24 (human) and 1.13 (mouse) compared with intact tissues (**Table 3**), but markers for proliferating SGCs (**Table 3**) were increased (by a median SSMD of 2.13 and 6.38 in humans and mice, respectively). Marker genes for all SGCs show a more mixed set of changes in both species since it is likely that the proportion of proliferating SGCs in culture gain at the expense of other SGC subpopulations (**Table 3**). The marker gene *CD68* for monocyte-derived immune cells also increases in humans (by 0.89, SSMD) and mice (by 3.25, SSMD) (**Table 3**).

Of the 49 literature sourced marker genes, 34 marker genes were validated by the Zeisel et al.'s data set. Of these, 5 SGC marker genes (*CATSPERZ*, *FBLN2*, *TYRP1*, *PRSS35*, and *FBLN5*) that were found to be expressed in Schwann cell and SGC subpopulations beside proliferating SGCs from the Zeisel et al. data set show a variety of changes between abundances in intact and cultured DRG. Benjamini-Hochberg-corrected *P* values (at the level of false discovery rate  $\leq 0.05$  based on the pre hoc list of 34 cell type enriched marker genes) in the human and mouse marker genes are consistent in trend and statistically significant for all remaining 29 genes in both species (except for *CD68* in humans which shows a consistent trend but higher within-group variability compared to its mouse ortholog; and *Col13a1* in mouse and *COL4A5* in human that show opposite trends in humans and mice possibly due to evolutionary gene regulatory divergence) (**Table 3**).

These changes happen broadly (as shown by the density function across pharmacologically relevant gene families, **Fig. 3**) and not just in specific regulatory pathways or gene sets. They indicate that the proportion of mRNA derived from neurons (and possibly Schwann cells) in our RNA-seq libraries decreases in cultured samples. In turn, this suggests that the proportion of neurons (which are postmitotic) to other cell types decreased in DRG cultures, while the proportion of dividing cells (such as fibroblast-like cells and proliferating SGCs) to other cell types

increased. However, Schwann cells, which can be mitotic and proliferate under certain conditions, potentially also decrease in proportion based on our data. This is likely because axonal contact is required for Schwann cell survival.<sup>69</sup> Developmentally established transcription factor expressions that define sensory neuronal identity (*PRDM12*, *TLX2*, *TLX3*, *POU4F1*, and *DRGX*) are all consistently decreased in human and mouse cultures (Supplementary file 1 sheets 1 and 2, available at <http://links.lww.com/PAIN/A983>), further suggesting that the observed changes are more likely to be caused by changes in relative proportions of cell types rather than molecular plasticity of neurons. These changes were expected, given the different mitotic statuses of these cell types, and were almost certainly the primary factors in distorting the transcriptome from what is seen in vivo. The zero-sum nature of our relative abundance measure (TPM) potentially also amplifies this signal.

### 3.5. Expression profiles of several pharmacologically relevant gene families show lower expression levels in dorsal root ganglion culture

A primary use of DRG cultures is to examine pharmacological effects of ligands for receptors with the assumption that this type of experiment reflects what occurs in vivo.<sup>38</sup> An underlying assumption of this type of experiment is that the presence or absence of a tested effect is reflected in consistent expression between in vivo and cultured conditions. To give insight into this assumption, we comprehensively cataloged expression of GPCRs, ligand-gated ion channels, and receptor kinases (RKs) in native and cultured human and mouse DRG. To comprehensively characterize the changes in these gene families, we also characterized expression profiles of non-RK soluble kinases (Supplementary file 1, sheets 3–10, available at <http://links.lww.com/PAIN/A983>). We limited our soluble kinase comparisons to a well-characterized subset with clear mouse to human orthologs.<sup>35</sup>

We find that a number of these genes are consistently detected in intact DRG but not in culture. This was seen in human gene families of GPCRs (detected in intact DRG: 292; in culture: 190; of which 176 were detected in both), ion channels (in intact DRG: 239, in culture: 179, in both: 172), RKs (in intact DRG: 68; in culture: 60; in both: 59), and non-RK kinases (in intact DRG: 286; in culture: 277; in both: 272), and a similar trend was observed in the mouse gene families as well. Since sensory neurons express a rich diversity of GPCRs and ion channels, the greater decrease in the number of consistently detected GPCRs and ion channels is likely the result of a proportional decrease of neurons in culture and/or decrease of gene expression in cultured neurons. Lists of consistently detected genes in these gene families are presented in Supplementary file 1, sheets 3–10, available at <http://links.lww.com/PAIN/A983>.

However, it is important to note that more than 75% of the human genes in these families (human: 679 of 885, mouse: 702 of 824) that are consistently detected in intact DRG are still detectable in culture. This suggests that at single cell resolution, DRG cultures could be used as a surrogate for in vivo models in preclinical research for a majority of pharmacologically relevant molecular assays.

Next, for genes that are consistently detected in at least one condition, we identified the ones in these gene families that have  $|SSMD| > 2.0$  (**Tables 4 and 5**, for human and mouse genes). Based on the SSMD values, while comparable numbers of GPCRs, ion channels and kinases were found to be decreased in cultured DRG (GPCRs—human: 85, mouse: 95; ion channels—human: 109, mouse: 122; kinases—human: 106, mouse: 70), more mouse genes were detected to be systematically trending in

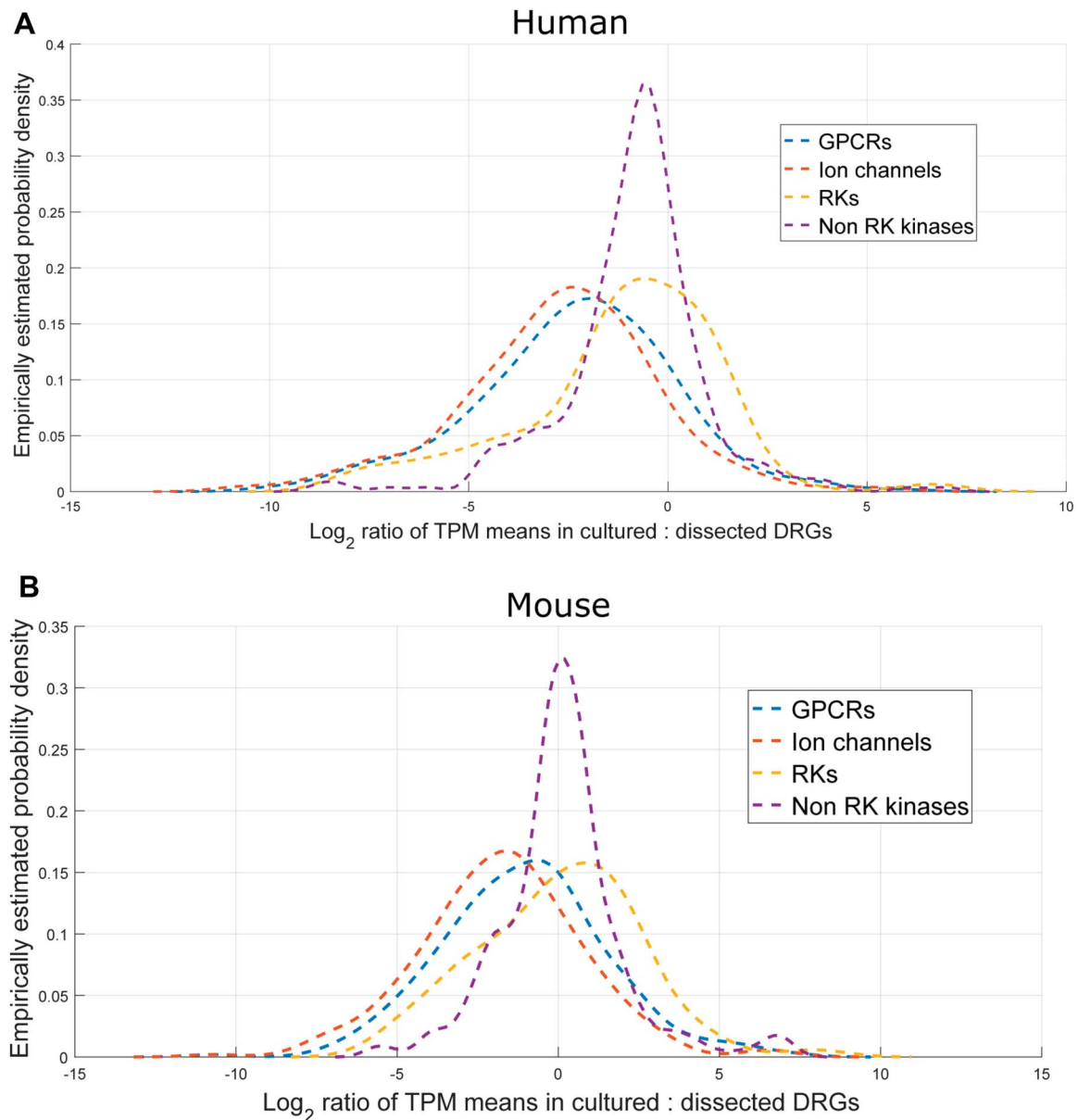


**Figure 3.** Empirical density distribution of log<sub>2</sub> fold changes (ratio of means) for GPCRs, ion channels, RKs, and non-RK kinases in human (A) and mouse (B). RKs and kinases as a group are weakly de-enriched in human and weakly enriched in mouse cultures (in the context of mean expression). However, both GPCRs and ion channels are strongly de-enriched in both human and mouse cultures, likely because of the variety of these genes that are expressed in sensory neurons. GPCR, G-protein-coupled receptor.

the opposite direction as compared to their human counterparts (GPCRs—human: 7, mouse: 20; ion channels—human: 7, mouse: 14; kinases—human: 22, mouse: 66). As noted before, within-group variation is likely lower in mice due to controlled laboratory conditions and similar genetic backgrounds, and this enables us to detect more expression changes that have smaller effect sizes (as in the case of genes that are increased in cultured conditions).

We also characterized the degree of change in expression by estimating the probability density of the fold change (ratio of means) for all the genes in these families. The empirically estimated probability density for the ratio of means (intact DRG:cultured DRG) of the human and mouse pharmacologically relevant genes (Fig. 3) shows a clear trend of decreased expression for a majority of the human ion channels and GPCRs.

Finally, we analyzed the trends in genes known to be involved in nociception, pain, and neuronal plasticity. Genes with ISSMDI > 2.0 between conditions, and known to be associated with pain from the Human Pain Genetics Database, and the Pain—Gene association gene set (from the Comparative Toxicogenomics Database in Harmonizome<sup>17,52</sup>), as well as from the literature, are underlined in Table 4. They identify pain-associated genes in these pharmacologically relevant families that change in expression between intact and cultured DRG. Based on changes in consistent detectability between the 2 conditions, ISSMDI values >2.0, or ratio of means >2.0, changes in expression of several genes are discussed below.

### 3.5.1. Changes in human G-protein-coupled receptors

Several GPCRs involved in proinflammatory pathways, including *CCR1*, *CCRL2*, *CNR1*, *CXCR4*, *F2R*, and *CHRM1*,<sup>71,74</sup> were found to

Table 4

Differentially expressed pharmacologically relevant genes (RKs boldfaced) in intact vs cultured human DRG with |SSMD| > 2, partitioned by mean TPM in condition of higher expression.

GPCRs		Ion channels		Kinases	
Up in native DRG (85)	Up in cultured DRG (7)	Up in native DRG (109)	Up in cultured DRG (7)	Up in native DRG (105)	Up in cultured DRG (22)
<b>&gt;50 TPM</b>					
<i>ADGRA2, ADGRB3, ADGRL1, ADGRL3, ADGRV1, GABBR1, GPR17, LGR5, LPAR6, and TACR2</i>	<i>GPR33</i> and <i>P2RY11</i>	<i>ANO5, AQP1, CACNA1A, CACNA1B, CACNA2D1, CACNA2D3, CACNB1, CACNB3, CLCN2, CLCN6, GRIK2, GRIN1, ITPR3, KCNQ2, P2RX3, PKD2L2, RYR1, RYR2, RYR3, SCN10A, SCN11A, SCN1B, SCN4B, SCN8A, SCN9A, TPCN1, TRPV1, and ZACN</i>	<i>CLIC1, CLIC4, P2RX4, and ANO6</i>	<i>BCR, BRAF, BRD2, BRSK2, CAMK1D, CAMK2A, CAMK2B, CAMK2G, CAMKK1, CDK10, CDK9, CDKL1, CLK1, CLK2, CLK4, CSNK1G2, DCLK2, ERBB3, FER, FGFR1, KALRN, KSR1, LIMK1, MAP2K5, MAP3K5, MAP3K6, MAPK12, MARK1, MARK2, MAST1, MAST2, MAST3, NEK1, NRBP2, NPR2, NTRK1, NTRK3, PINK1, PRKACA, PRKCA, PRKCZ, RET, ROCK2, SPEG, SRPK2, TAF1, TGFBR2, TLK2, TRRAP, TYRO3, ULK2, ULK3, and WNK1</i>	<i>ABL2, AXL, CDK2, CDK4, DAPK3, ILK, MAPKAPK2, MYLK, NRBP1, PDGFRB, PTK7, and TRIO</i>
<b>&gt;25 TPM</b>					
<i>ADGRB1, ADGRG2, CELSR2, GABBR2, GPR18, GPR183, and MRGPR</i>	<i>ADGRF5</i> and <i>ADGRL4</i>	<i>ANO3, ANO8, AQP11, CACNA1C, CACNA1D, CHRNAZ, CHRNE, CLCN5, GABRA2, GABRB3, GRIA4, GRIK3, GRIK5, HCN2, MCOLN3, SCN1A, and TRPM2</i>	<i>KCNN4</i>	<i>BMPR2, DCLK1, EGFR, HIPK2, HSPB8, LRRK1, LRRK2, MAPK11, MST1, NTRK2, PAK3, PRKACB, PRKCB, PRKCE, PRKCI, SLK, TSSK3, TSSK4, TTBK2, TTN, and ULK1</i>	<i>DYRK4, FLT1, MAPKAPK3, and MELK</i>
<b>&gt;12.5 TPM</b>					
<i>CCR10, CHRM5, CXCR6, GNRHR, GPR146, GPR171, GPR37L1, GPR62, GPRC5B, GRM7, HTR2B, OR10AD1, OR2A1, OR2A42, OR52B6, P2RY12, P2RY14, SSTR1, TAS1R3, and TAS2R40</i>	<i>CXCR4</i>	<i>ANO4, ASIC1, CACNB2, CACNB4, CACNG7, CHRNB1, CLCN4, GABRG2, GJA9, GLRB, GRIA2, GRIK1, GRIN3B, KCNC1, KCND1, KCNH2, KCNQ5, KCNT2, LRRC8B, NALCN, P2RX5, P2RX6, and SCN11D</i>	<i>AQP9</i>	<i>ACVR2A, ADCK1, BRD3, CDKL2, DAPK2, DSTYK, EPHA5, EPHA6, EPHB3, EPHB6, MAK, MAP2K6, MUSK, MYT1, OBSCN, POMK, PRKX, TNK1, TTBK1, and WNK2</i>	<i>IRAK2, PLK1, TRIB3, and TTK</i>
<b>&gt;6.3 TPM</b>					
<i>AVPR2, CELSR3, F2RL2, FZD2, GPER1, GPR158, GPR162, GPR182, GPR82, GPR87, GRM4, LPAR3, OPRM1, OR1K1, OR2A7, OR3A3, OR51I2, OR51J1, OXER1, PTGER4, TAS2R39, and TSHR</i>	—	<i>ANO2, CFTR, CHRG, CLIC3, GJA4, GJB7, GJC3, GRIN2B, HCN1, KCNA2, KCNH7, KCNH8, KCNK12, KCNN2, KCNS1, LRRC8D, and SCN3B</i>	—	<i>EPHA10, FLT3, HIPK4, LMTK2, NEK5, PNCK, and STKLD1</i>	<i>NEK2</i>
<b>&gt;3.1 TPM</b>					
<i>GPR149, GPR45, GRM3, GRM6, MRGPRF, OR11L1, OR13J1, OR5C1, OR6F1, OR6V1, and PTPN13</i>	<i>GPR176</i> and <i>F2R</i>	<i>AQP12B, GJB3, GRIN3A, KCNB2, KCNH1, KCNH3, KCNH6, KCNJ3, KCNK1, KCNK15, and TRPC5</i>	—	<i>KSR2</i> and <i>PRKAA2</i>	<i>DYRK3</i>
<b>≤3.1 TPM</b>					
<i>ADRA2C, CCKBR, CXCR3, GPR135, GPR179, GPR26, GRM8, HTR5A, HTR6, OPRL1, OR1Q1, OR2AE1, OR5AS1, SSTR2, and TBXA2R</i>	—	<i>GLRA3, HCN3, KCNK10, KCNH5, KCNJ10, KCNJ12, KCNJ5, KCNJ9, KCNQ4, KCNV1, LRRC8E, SCN2B, and TRPC3</i>	<i>KCNJ8</i>	<i>FRK</i> and <i>PRKCO</i>	—

The number of genes in each column is shown in parentheses. Genes known to be associated with pain from genome wide association study/functional association databases and the literature are underlined. Typically, smaller TPM brackets have higher technical variance.

DRG, dorsal root ganglia; GPCR, G-protein-coupled receptor; TPM, transcripts per million; SSMD, standardized mean difference.

**Table 5**

**Differentially expressed pharmacologically relevant genes (RKs boldfaced) in intact vs cultured mouse DRG, with |SSMD| > 2 partitioned by mean TPM in condition of higher expression.**

GPCRs		Ion channels		Kinases	
Up in native DRG (95)	Up in cultured DRG (20)	Up in native DRG (122)	Up in cultured DRG (14)	Up in native DRG (70)	Up in cultured DRG (66)
<b>&gt;50 TPM</b>					
<i>Adora1, F2n2, Gabbr1, Gabbr2, Gpr137, Lpar3, and Mrgprd</i>	<i>Adgra5, Mrgprf, and Smo</i>	<i>Ano3, Asic1, Asic2, Asic3, Cacna1a, Cacnb1, Cacnb3, Cacng7, Clcn2, Clcn6, Gabrg2, Glr3, Grik1, Grik5, Grin1, Hcn2, Htr3a, Kcna2, Kcnc4, Kcnd1, Kcnk1, Kcns1, Kcns3, Kcnt1, Mcoln1, Scn10a, Scn11a, Scn1b, Scn4b, Tpc3, Trpm4, and Trpv1</i>	<i>Clic1, Clic4, Gja1, Kcnn4, and Lrrc8c</i>	<i>Akt3, Brsk1, Brsk2, Camk2a, Camk2b, Camk2g, Cdk10, Cdk5, Cdkl2, Kit, Limk1, Limk2, Map2k4, Mapk11, Mapk12, Mast1, Nek1, Nek7, Npr2, Nrpo2, Ntrk1, Ntrk2, Phkg2, Pim3, Pink1, Prkaca, Prkacb, Prkac, Prkcb, Prkcd, Prkce, Prkcq, and Prkcz</i>	<b>Acvr1, Aurka, Aurkb, Axl, Bckdk, Bmpr1a, Cdk4, Ddr1, Erbb3, Ilk, Mapkapk2, Mark3, Pak2, Pbk, Pdgfrb, Plk1, Plk2, Riok3, Rock2, Ryk, and Srm</b>
<b>&gt;25 TPM</b>					
<i>Adgrb1, Cysltr2, Gpr45, Gprc5c, Gm7, Htr1d, P2ry1, Ptgd, and Pth1r</i>	<i>Adgra2, Fzd1, and Fzd2</i>	<i>Ano8, Cacna1h, Cacna2d3, Chna6, Chnb2, Gabrb3, Gria4, Hcn3, Kcnb1, Kcnc1, Kcnc3, Kcnj12, Kcnn1, Kcnq4, Tpcn1, and Trpa1</i>	<i>Gjc1, Kcnk5, and Pkd2</i>	<i>Acvr1b, Camk1g, Dclk3, Mark1, Myt1, Ntrk3, Pim2, Pnck, and Ttbk1</i>	<i>Abl1, Bub1, Cdk2, Cdk7, Ddr2, Ephb2, Ephb3, Erbb2, Map3k3, Melk, Met, Nek2, Peak1, Pkd2, Pkn2, Plk4, Prag1, Ripk1, Ripk3, Tec, Tgfb1, and Tgfb2</i>
<b>&gt;12.5 TPM</b>					
<i>Adgrb2, Adgrg2, Adra2c, Agr1a, Cckar, Cxcr4, Gpr161, Gpr162, Gpr27, Gpr35, Gm4, Mrgpra2a, Mrgpra2b, Mrgprx1, Noy2r, Opn3, Opr1, Ptger1, and Ptgr</i>	<i>Ackr3, Fzd7, and S1pr2</i>	<i>Cacna2d2, Cacng5, Chna3, Chna7, Gabra1, Gabra2, Grik4, Htr3b, Kcnb2, Kcng2, Kcnh1, Kcnh6, Kcnk2, Kcnk3, Kcnk4, Kcnm2, P2rx6, Scn1a, Scn2b, and Tipm2</i>	<i>Clcn5</i>	<i>Camk1d, Camkk1, Dapk2, Flt3, Lmtk3, Map3k5, Pdk1, and Wnk2</i>	<i>Cdc7, Cdk6, Ephb4, Fer, Haspin, Irak4, Jak2, Lyn, Mastl, Mki, Pask, Riok1, Rock1, Scyl3, Trib3, Tik, Vrk1, Vrk2, and Wee1</i>
<b>&gt;6.3 TPM</b>					
<i>Adora2a, Chrm4, Cnr1, Gpr135, Gpr139, Gpr146, Gpr149, Gpr157, Gpr37, Gpr61, Gpr75, Gm8, Hcrr1, Htr1b, Htr7, Lgr5, Lpar5, Prokr1, Ptger3, Ptger4, and Sstr2</i>	<i>C3ar1, C5ar1, Celsr1, Cmktr1, Fzd6, and Lpar6</i>	<i>Aqp11, Cacna1d, Cacng2, Cacng4, Chmb3, Chmb4, Gabra3, Gabrg1, Gjb6, Gria1, Grin3a, Hcn4, Kcna4, Kcnc2, Kcng4, Kcnh7, Kcnj11, Kcnj3, Kcnj4, Kcnq3, Kcnq5, Kcnu1, Kcnv1, Nalcn, P2rx2, P2rx5, Ryr2, Trpc6, and Trpm8</i>	—	<i>Amhr2, Cdkl1, Mst1r, Prkaa2, and Tiet</i>	<i>Ikke and Map3k2</i>
<b>&gt;3.1 TPM</b>					
<i>Chrm2, Crhr2, Gpr156, Gpr160, Gpr22, Gpr3, Gpr68, Hcrr2, Hrh3, Htr1a, Htr4, Nmur1, Ntsr2, and Pitpnm3</i>	<i>Adra1b, F2r11, and P2ry6</i>	<i>Cacna1i, Gria2, Kcnk18, and Scn5a</i>	<i>Gjb5 and Lrrc8e</i>	<i>Brd1, Camk4, Eph10, Ksr2, Npr1, and Tek</i>	<i>Ror1</i>
<b>≤3.1 TPM</b>					
<i>Adrb1, Ccr10, Ccr2, Chrm1, Crhr1, Galr1, Gpr150, Gpr174, Gpr179, Gpr182, Gpr21, Gpr26, Gpr62, Gpr83, Gpr88, Hcar1, Hrh2, Htr5a, Lhcg, Mas1, Oprd1, Oprk1, Ptafr, Ptger2, and Rho</i>	<i>Ccr5 and Gpr84</i>	<i>Aqp4, Best1, Cacna1e, Cacng3, Chna10, Chna4, Clic5, Gabrb1, Gabrb2, Gjd2, Kcnd2, Kcng1, Kcng3, Kcnh5, Kcnj13, Kcnj14, Kcnj16, Kcnj2, Kcnj8, Kcnj9, Kcnn3, Kcns2, and Scn1a</i>	<i>Chrna1, Gjb4, and Itpr2</i>	<i>Bmx, Cdkl4, Eph6, Eph8, Ephb1, Insrr, Itk, Nek11, and Sbk3</i>	<i>Frk</i>

The number of genes in each column is shown in parentheses. Typically, smaller TPM brackets have higher technical variance. DRG, dorsal root ganglia; GPCR, G-protein-coupled receptor; TPM, transcripts per million; SSMD, standardized mean difference.

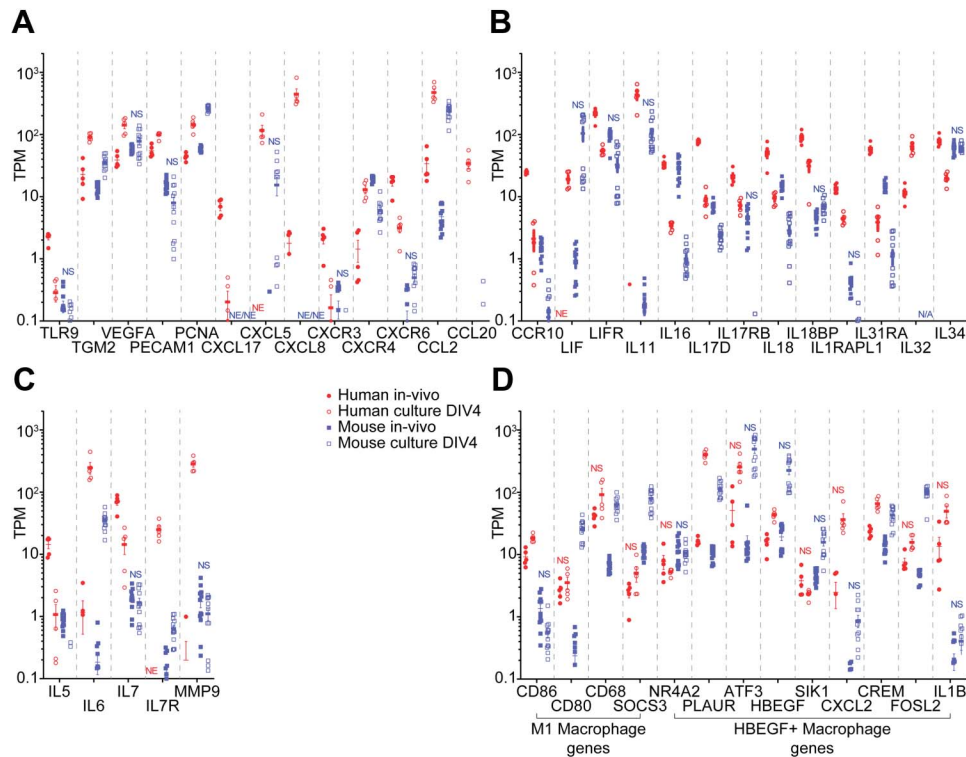


**Figure 4.** Expression levels in human and mouse intact vs cultured DRG. A wide diversity of genes involved in inflammation and proliferation, nerve and neuronal injury and repair, and immune signaling and response are profiled (A–C). Key expressed genes for M1 macrophages and *HBEGF*+ macrophages are also shown (D). DRG, dorsal root ganglia; NS,  $|\text{ISSMD}| \leq 2$ ; NE, not consistently detected for that condition; N/A, not applicable because orthologous gene not identified in that species; SSMD, strictly standardized mean difference.

increase in abundance in cultured DRG. G-protein-coupled receptors found to be decreased in culture included *DRD5*, *HTR5A*, *HTR6*, and some metabotropic glutamate receptors (*GRMs*) such as *GRM4* and *GRM7*, all of which have been shown to be highly neural tissue-enriched in humans (based on neural proportion score  $>0.9$  in Ray et al.<sup>51</sup>). Their mouse orthologs have also been shown to be neuronally expressed in DRG single-cell RNA-seq experiments.<sup>61</sup> Many of these and other GPCRs changing in abundance between intact and cultured DRG (Table 4, and Supplementary file 1, sheet 3, available at <http://links.lww.com/PAIN/A983>) have been noted as potential targets for pain treatment.<sup>8,16,37,55</sup> Therefore, our findings suggest that under certain culture conditions false negatives could arise for these targets.

### 3.5.2. Changes in mouse G-protein-coupled receptors

Proinflammatory mouse GPCRs were also found to be increased in cultured DRG, including *Ccr5*, *Cxcr6*, *F2r*, and *F2rl1*.<sup>30,59,63</sup> Several neuronally expressed mouse GPCRs (based on Usoskin et al.<sup>61</sup>), including *Chrm2*, *Htr1a*, *Htr2c*, *Htr7*, and metabotropic GRMs such as *Grm4*, showed higher expression in intact DRG (Table 5, and Supplementary file 1, sheet 4, available at <http://links.lww.com/PAIN/A983>). Many of these genes in the human and mice data sets were from orthologous families of receptors, including cytokine receptors, the protease activated receptor family (*F2R*), 5-HT receptors, and metabotropic GRMs.

### 3.5.3. Changes in human ion channels

Among the ion channels increased in abundance in cultured DRG were the chloride intracellular channels *CLIC1* and *CLIC4*, gap junction protein *GJA1*, *KCNQ1* ( $K_{\text{v}}6.1$ ), *KCNJ8* ( $K_{\text{IR}}6.1$ ), *KCNN4*

( $K_{\text{Ca}}4.2$ ), and *P2RX4*, *TRPV4*, and voltage-dependent anion channels *VDAC1* and *VDAC2*. Interestingly, many of these ion channels are involved in membrane potential hyperpolarization, suggesting a potential compensatory mechanism to suppress excitability. Neuronally expressed voltage-gated calcium channels such as *CACNA1B*, *CACNA1F*, *CACNA1I*, *CACNAG5*, *CACNAG7*, and *CACNAG8*; glutamate ionotropic receptors *GRIA2* and *GRIN1*; voltage-gated potassium channels *KCNA1*, *KCNA2*, *KCNB2*, *KCNC3*, *KCND1*, *KCND2*, *KCNH2*, *KCNH3*, *KCNH5*, *KCNJ12*, *KCNK18*, *KCNQ2*, *KCNT1*, and *KCNV1*; purinergic receptors *P2RX2* and *P2RX5*; and voltage-gated sodium channels *SCN1A*, *SCN4A*, *SCNN1A*, and *SCNN1D* were found to be increased in intact DRG (Table 4, and Supplementary file 1, sheet 5, available at <http://links.lww.com/PAIN/A983>).

### 3.5.4. Changes in mouse ion channels

Changes in mouse ion channel genes were also quantified (Table 5, and Supplementary file 1, sheet 6, available at <http://links.lww.com/PAIN/A983>). Genes increased in DRG cultures included several of the same families seen in human, such as chloride intracellular channels *Clic1* and *Clic4*; gap junction proteins *Gja1*, *Gja3*, *Gjb3*, *Gjb4*, *Gjb5*, and *Gjc1*; the glutamate ionotropic receptor *Grik3*; voltage-gated potassium channels *Kcnk5* ( $K_{\text{2p}}5.1$ ) and *Kcnn4* ( $K_{\text{Ca}}4.2$ ); and purinergic receptors *P2rx1* and *P2rx7*. Among ion channels decreased in culture were the chloride intracellular channels *Clic3* and *Clic5*; voltage-gated calcium channels *Cacna1i*, *Cacna1s*, and *Cacng3*; cholinergic receptors *Chrna10*, *Chrna6*, *Chrbn3*, and *Chrbn4*; glutamate ionotropic receptors *Grik1* and *Grin2c*; 5-HT

receptors *Htr3a* and *Htr3b*; voltage-gated potassium channels *Kcnd2*, *Kcng3*, *Kcng4*, *Kcnj11*, *Kcnj13*, *Kcnn1*, *Kcnn2*, and *Kcns1*; *P2rx2*; voltage-gated sodium channels *Scn1A* and *Scn11A*; and TRP channels *Trpm2* and *Trpm8*. Most of these genes are well known to be neuronal in expression.<sup>61</sup> Overall, the ion channel subfamilies changing in expression in culture in both species were similar and included primarily voltage-gated calcium/potassium/sodium channels, purinergic receptors, and gap junction proteins.

### 3.5.5. Changes in human RKs and other kinases

We found that the neuronally expressed genes from the *NTRK* family (*NTRK1*, *NTRK2*, and *NTRK3*) and the *CAMK* family (*CAMK1D*, *CAMK1G*, *CAMK2A*, *CAMK2B*, *CAMK2G*, and *CAMKK1*) were decreased in culture in the human DRG (Table 4, and Supplementary file 1, sheets 7 and 9, available at <http://links.lww.com/PAIN/A983>).

### 3.5.6. Changes in mouse RKs and other kinases

Consistent with what we found in the human cultures, we identify decrease in abundance in neuronally expressed *Ntrk* family (*Ntrk1*, *Ntrk2*, and *Ntrk3*) and *Camk* (*Camk1g*, *Camk2a*, and *Camk2b*) family genes. The changes in the *Ntrk* family, responsible for neurotrophin signaling in adult DRG neurons, demonstrate a consistent interspecies trend in culture. Consistent trends in the *Camk* family genes, which play a vital role in  $Ca^{2+}$ -dependent plasticity in the brain<sup>14</sup> and in nociceptors,<sup>10,11,21</sup> also show conserved patterns in the DRG cultures (Table 5, and Supplementary file 1, sheets 8 and 10, available at <http://links.lww.com/PAIN/A983>).

### 3.6. Neuronal injury and inflammation markers were increased in human and mouse dorsal root ganglion cultures

Dissection of the DRG causes an axotomy that may induce an inflammatory phenotype as is seen in vivo after peripheral nerve injury.<sup>42</sup> As shown in Figure 4, many genes associated with inflammation and cell proliferation, neuronal injury and repair, and immune signaling and response, including cytokines<sup>1,9,66</sup> and matrix metalloproteases<sup>29</sup> associated with neuropathic pain, were differentially expressed in human and mouse DRG cultures with respect to intact DRG.

Since several of these genes are increased or decreased in cultured samples, we used the mouse DRG single cell RNA-seq profiles<sup>61</sup> to putatively identify cell types of expression among cells constituting the DRG (Supplementary file 1, sheet 11, available at <http://links.lww.com/PAIN/A983>). Indeed, we find that genes primarily expressed in neurons and Schwann cells decrease in relative abundance, even if they are involved in proinflammatory signaling, since it is likely that these cell types are reduced in frequency in DRG cultures. Interestingly, several genes predicted to be primarily expressed in immune cells (*TLR9* and *CXCR3*) (Fig. 4A) and in vascular cells such as *IL18BP* (Fig. 4A) and *CXCL17* (Fig. 4B) were found to be reduced in relative abundance in cultures, suggesting that potential increase in immune and vascular cell proportions in culture are limited to certain cell subtypes in these categories. As maximal examples of gene expression changes in our data sets, *IL6* and *MMP9* mRNA expression were increased 100-fold or more in human DRG culture (Fig. 4C).

Multiple subtypes of macrophages are involved in inflammatory processes and can be identified with specific markers.<sup>24</sup> In

human and mouse, key M1 macrophage genes *CD68*, *CD80*, and *SOCS3* were all upregulated in culture compared with intact ganglia. As identified in a recent study, HBEGF+ inflammatory macrophages are responsible for fibroblast invasiveness in rheumatoid arthritis patients.<sup>31</sup> We noted that multiple genes expressed in this specific subtype of macrophage (*PLAUR*, *HBEGF*, and *CREM*) were increased in human and mouse DRG cultures, suggesting that this particular subtype of macrophage may be present in DRG cultures from both species (Fig. 4D).

While specifically identifying the exact subtype of immune cell involved is outside the scope of our bulk RNA-sequencing assay, our findings reveal clearly that many genes involved in neuronal injury, cell proliferation and inflammation, and immune signaling and response are increased in DRG cultures.

### 3.7. Similarities and differences between human and mouse dorsal root ganglion culture transcriptomes in the context of intact dorsal root ganglion transcriptomes

Complicated orthologies and differential evolutionary dynamics between human and mouse gene families,<sup>72</sup> and gaps in human to mouse orthology annotation,<sup>41</sup> make comparative transcriptomic comparisons difficult between human and mouse transcriptomes. We have previously made similar comparisons between native human and mouse intact DRG<sup>51</sup> not only finding overall similarities but also some changes in gene expression. Since we are analyzing changes in expression at the level of individual genes (such as pharmacologically relevant ones), we limited our analysis to changes in expression in GPCRs, ion channels, and kinases in DRG cultures for tractability.

We calculated trend scores for each GPCR, ion channel, RK, and non-RK kinase, after eliminating genes from the analysis with complicated orthologies between humans and mouse (Supplementary file 1, sheets 12-15, available at <http://links.lww.com/PAIN/A983>). We find a weak correlation between trend scores of human genes and their mouse orthologs in GPCRs (Pearson's *R*: 0.19, one-tailed test *P* value: 0.0008) and ion channels (Pearson's *R*: 0.15, one-tailed test *P* value: 0.012). For specific genes, we find consistent increased (eg, *F2R*, *GPRC5A*, and *TRPV4*) or decreased (eg, *SCN* subfamily members, *GABAR* subfamily members) in cultured samples for both species. This suggests that expression patterns across cell types, which potentially contributes to the trend scores, are likely conserved in these genes across species. However, in several cases, genes may not be consistently detectable in one species but present in one or more conditions in the other (eg, *CHRM5* only detectable in human DRG, *CHRN4* only detectable in mouse DRG). *TRPC5* is expressed at low levels in 3 intact mouse DRG samples, but significantly increased in expression in all human samples. In addition, several genes are expressed in both species, but have opposing expression trends across intact and cultured DRG (eg, *ACKR4* and *CXCR6* decreased in human cultures, but increased in mouse cultures). Such changes are likely due to evolutionary divergence between species in gene expression across cell types, and/or differential transcriptional regulation between species. Both of these involve regulatory evolution.

Supplementary file 1, sheets 12-15, available at <http://links.lww.com/PAIN/A983>, profile members of these gene families, their trend scores, and the number of human and mouse samples where they are detectable. This provides a roadmap for identifying genes changing in cultured vs intact DRG across species and creates a resource for the neuroscience community interested in performing molecular assays in cultured DRG on these genes.

Since several members of the MRGPR family do not have a one-to-one orthology between human and mouse genes, they were not included in the trend score calculation tables (Supplementary file 1, sheet 12, available at <http://links.lww.com/PAIN/A983>). Transcripts per million values from human and mouse cultures for all members of this gene family are presented in their own table because this family of genes plays an important role in sensory neuroscience (Table 6).

### 3.8. *Cd68* expression profiling using RNAscope

Previous mammalian DRG culture protocols for profiling RNA landscapes in sensory neurons have used mitotic suppressors to inhibit proliferation of mitotic cells<sup>57</sup> despite evidence that such inhibitors produce off-target effects on neurons.<sup>64</sup> This lends support to our hypothesis that changes to the cultured DRG transcriptome are at least partly shaped by an increase in proportion of proliferative cells.

We chose to profile *Cd68* by RNAscope. The gene product for *Cd68* is well known as a marker for myeloid lineage immune cells such as monocytes and macrophages, including tissue-residential and circulating myeloid cells (microglia/macrophage) in the mouse CNS<sup>75</sup> and DRG.<sup>32</sup>

RNAscope assays were conducted in intact mouse DRG (Fig. 5A). Gene expression for *Cd68*, and *Calca* (marker for most nociceptive neuronal subpopulations) and *P2rx3* (marker for most nonpeptidergic nociceptive neuronal subpopulations), was detected

using the RNAscope probes. In addition, immunostaining of Nf200 (gene product of *Nefh*, marker for neurofilament cell bodies and afferents) was performed. We also performed RNAscope assays in cultured mouse DRG (Fig. 5B) using only the *Cd68* probe identifying *Cd68* gene expression, additionally immunostaining Peripherin (gene product of *Prph*—a pan-sensory neuronal gene marker).

We then queried the mousebrain.org<sup>75</sup> database to identify putative cell type of expression (Fig. 5C) of *Cd68*. The database contained gene expression levels for neurofilament (PSNF1-3), peptidergic (PSPEP1-8), and nonpeptidergic (PSNP1-6) sensory neuronal subpopulations as well as Schwann cell (SCHW) and SGC (SATG1-2) subpopulations. Since the database did not profile DRG vascular or immune cells, we used CNS vascular and immune cell population gene expression profiles as surrogate. Central nervous system vascular cells profiled include venous/capillary/arterial endothelial cells (VECA, VECV and VECC), vascular leptomeningeal cells (ABC and VLMC1-2), pericytes (PER1-3), and arterial smooth muscle cells (VSMCA). Central nervous system immune cells profiled include microglia/tissue-resident macrophages (MGL1-3) and perivascular macrophages (PVM1-2). We thus find (using an external data set) that *Cd68* expression in mouse DRG is non-neuronal, and that it is only expressed in macrophage-like cell populations, in agreement with DRG immune cell studies.<sup>32</sup>

Overlays of fluorescence imaging of the intact DRG (Fig. 5D) and cultured DRG (Fig. 5E, additionally overlaid with DAPI stain to identify nuclear DNA) on the 20X objective show cofluorescence among the cell type markers. Little to no overlap is seen between

**Table 6**

#### MRGPR/Mrgpr family gene expression levels in human and mouse.

Human			Mouse		
Gene name	Mean TPM in intact DRG	Mean TPM in cultured DRG	Gene name	Mean TPM in intact DRG	Mean TPM in cultured DRG
MAS1	0.02	0.06	<i>Mas1</i>	0.75	0.05
MAS1L	0.0	0.0	No <i>MAS1L</i> ortholog	—	—
MRGPRD	0.85	0.21	<i>Mrgpra1</i>	0.77	0.04
MRGPRE	31.41	1.53	<i>Mrgpra2a</i>	20.91	0.67
MRGPRF	5.45	1.84	<i>Mrgpra2b</i>	23.85	0.96
MRGPRG	0.00	0.00	<i>Mrgpra3</i>	24.50	0.02
MRGPRX1	4.45	0.48	<i>Mrgpra4</i>	0.48	0.01
MRGPRX2	0.00	0.00	<i>Mrgpra6</i>	0.00	0.00
MRGPRX3	0.32	0.08	<i>Mrgpra9</i>	0.98	0.01
MRGPRX4	0.12	0.00	<i>Mrgprb1</i>	0.15	0.03
			<i>Mrgprb2</i>	0.09	0.00
			<i>Mrgprb3</i>	0.00	0.00
			<i>Mrgprb4</i>	7.33	0.00
			<i>Mrgprb5</i>	9.14	0.04
			<i>Mrgprb8</i>	0.02	0.00
			<i>Mrgprd</i>	74.20	0.03
			<i>Mrgpre</i>	21.22	19.68
			<i>Mrgprf</i>	7.91	73.72
			<i>Mrgprg</i>	0.00	0.00
			<i>Mrgprh</i>	0.23	0.04
			<i>Mrgprx1</i>	18.86	0.82
			<i>Mrgprx2</i>	0.04	0.01

DRG, dorsal root ganglia; TPM, transcripts per million.

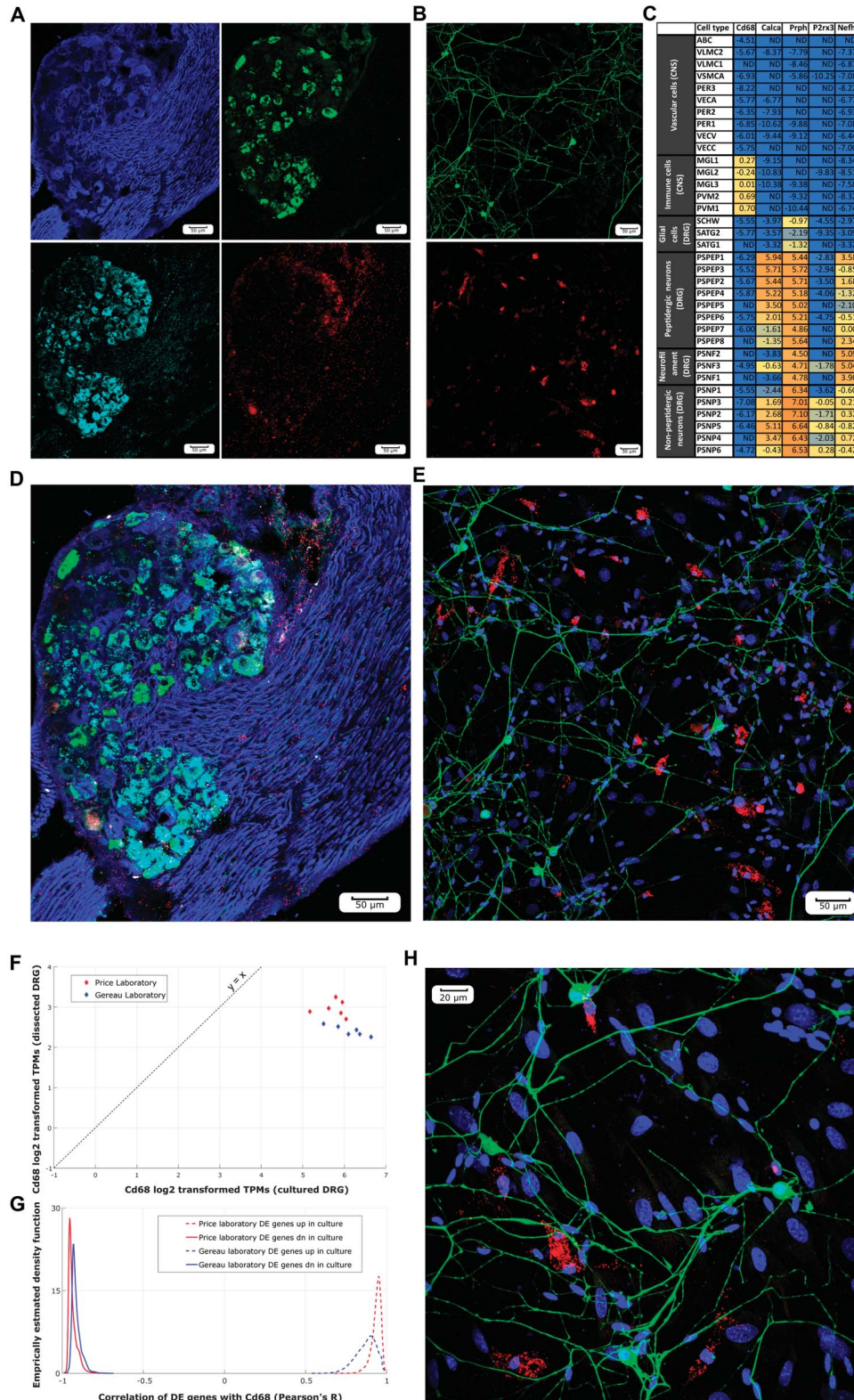


**Figure 5.** *Cd68* expression in intact vs cultured mouse DRG. RNAscope in situ hybridization imaging (20×) in pseudocolor for *Cd68* (red) in combination with various neuronal markers including *Calca* (green), *P2rx3* (cyan), and immunostained Nf200 (blue) in intact mouse DRG (A). RNAscope in situ hybridization imaging (20×) in pseudocolor for *Cd68* (red) and immunostained Peripherin (green) and DAPI staining (blue) in cultured mouse DRG (B). log2 transformed expression levels of *Cd68* and neuronal markers from mousebrain.org (C) in mouse DRG neuron and glial subtypes, and nervous system vascular and immune cells show *Cd68* is detected only in macrophage-like cells (ND, not detectable). Overlay of images show that *Cd68* mRNA is not expressed in neurons in either intact (D) or cultured (E) mouse DRG neurons. Expression levels (in log2-transformed TPMs) of *Cd68* in intact vs cultured mouse DRG are plotted (F) to show the consistent increase of *Cd68* expression in cultures. Differentially expressed gene TPMs show strong correlation (or anticorrelation) to *Cd68* abundance (in TPMs) (G), suggesting a consistent phenotype across samples and laboratories. Overlay of RNAscope in situ hybridization imaging (40×) for cultured mouse DRG (H) suggests *Cd68*+ cells have consistent shape and size with respect to DRG macrophages. Scale bar for 20× images equal to 50 μm and 40× equal to 20 μm. DRG, dorsal root ganglia; TPM, transcripts per million.

*Cd68*-driven fluorescence and the neuronal markers in intact DRG, clearly showing that *Cd68* expression is non-neuronal in origin. In the cultured DRG, we find no overlap of *Cd68*-driven fluorescence and Peripherin staining.

It is well documented that macrophage accumulation occurs in the DRG in mouse models of neuroinflammation,<sup>33</sup> and macrophages are also known to upregulate *Cd68* expression in response to inflammatory stimuli.<sup>13</sup> Looking at the RNA-seq libraries we generated, we find that *Cd68* expression is consistently increased in both Price and Gereau laboratory mouse cultured DRG data sets (Fig. 5F). In conjunction with the RNAscope data, this suggests that either *Cd68*+ macrophages increase in proportion in culture, or gene expression of *Cd68* increases in macrophages in culture, or a combination of both occurs.

We then chose all the genes that were identified as differentially expressed between intact and cultured mouse DRG based on our differential expression criteria (Supplementary file 1, sheet 2, Column AR, available at <http://links.lww.com/PAIN/A983>), which include *Cd68*. For both the Price and Gereau laboratory data sets, expression levels of these genes were tested for correlation with *Cd68* expression levels (Fig. 5G) showing strong correlation of *Cd68* with genes that increased in relative abundance in culture, and strong anticorrelation with genes that decreased in relative abundance in culture. This is also in agreement with our hypothesis of increase in cell type proportions of mitotic cells at the expense of sensory neurons (and possibly Schwann cells). The increased spread of correlation coefficients of genes increasing in Gereau laboratory mouse cultures (with respect to Price laboratory data sets) is in agreement with greater variability in *Cd68* expression (in TPM) in Gereau laboratory cultures (SD = 19.3) compared with Price laboratory cultures (SD = 10.9).

Using the 40× objective (Fig. 5H), we further find that the size and shape of *Cd68*+ cells are commensurate with previous studies of DRG macrophages.<sup>73</sup> The evidence, in its entirety, points to changes in constituent cell type proportions in DRG cultures, with potential increase of frequency of macrophage-like cells in DRG cultures.

#### 4. Discussion

We are unaware of any previous studies that have used genome-wide technologies to characterize transcriptomes between intact and cultured DRG. Although in vivo cross-species comparisons have previously been made,<sup>51</sup> in vitro transcriptome comparisons between mice and human DRG have not been performed, despite the obvious need for such knowledge given the reliance on the mouse model for both target and drug discovery work in the pain area.<sup>16,38,50,62,76</sup> Certain perturbation studies<sup>47</sup> such as gene expression knockdowns, DNA editing, or optogenetic optimization,<sup>39</sup> especially in the context of human research, cannot be performed in vivo, causing DRG cultures to be essential to human, clinical translational research. Our work gives fundamental new insight into some of the most commonly used model systems in the pain field with important implications for future work.

We reach 2 major conclusions. First, although many pharmacologically meaningful features of the DRG are well-conserved from mouse to human, there are some important differences that need to be considered in future experimental design. Moreover, there are a small but potentially important number of human receptors that simply cannot be studied in culture systems that may be good targets for drug discovery. Second, mouse and human DRG cultures take on an inflammatory-like transcriptomic

phenotype that shares some qualities with transcriptomic changes in neuropathic pain.<sup>1,29,34,43</sup> Therefore, the cultured DRG system may reflect certain clinical features that would be advantageous for neuropathic pain mechanism and/or drug discovery, especially in humans where these samples are not readily available except under very unique circumstances.<sup>43</sup> In further support of this conclusion, we find a subset of genes that are upregulated in cultures from mouse and human DRG that are consistent with a transcriptional reprogramming of sensory neurons after axonal injury that is associated with some aspects of neuropathic pain.<sup>40</sup>

A critique of using primary neuronal cultures to test pharmacological targets is that cultures are not an accurate representation of native tissue. Although there were some specific genes that did not appear in culture when compared with native tissue and vice versa, the main difference between the 2 conditions was in the expression level of each gene, which our data strongly suggest is due to change in the proportion of cell types. Specifically, the proportion of neurons in culture was decreased when compared with macrophages, fibroblast-like cells, and SGCs. To this end, when specific pharmacological targets are being tested in either mouse or human cultures, it is important to check that these targets remain expressed and our work provides a comprehensive resource to do this in both species (Supplementary file 1, available at <http://links.lww.com/PAIN/A983>). Because pharmacology is the most common use of cultured DRG, we focused our analysis on pharmacologically relevant targets. Interestingly, both mouse and human cultures displayed an increase in M1 and HBEGF+ macrophage<sup>31</sup> markers when compared with native tissue. This change suggests an increase in the inflammatory macrophage population in culture. We predict that this shift is due to phenotypic shifts and/or increased cell type proportion of tissue resident macrophages caused during the dissociation and culturing process, potentially replicating a nerve injury phenotype.<sup>1,9,28,29,66</sup> The presence of these cell types in culture could be used to further study how macrophages and sensory neurons interact and should be very relevant to the pain community.

Families of genes remained consistently expressed in both species following dissociation and culturing protocols, but individual genes of the same family varied in whether they were present in either mouse or human. For example, *Kcna1* was consistently detected only in mouse DRG cultures. Therefore, although most ion channel types are likely to be equally represented in both human and mouse DRG neurons, there is a substantial chance that the specific subtypes of channels that make up those conductances will be different between species, and such changes may be present both in vivo and in culture. In fact, studies focusing on exactly this question for voltage-gated sodium channels in DRG between rat and human have found qualitative similarities but key differences that are almost certainly due to differences in expression between species.<sup>76</sup> This is a critical distinction for pharmacology because a primary goal in therapeutic development is ion channel subtype specific targeting.<sup>50</sup> It is vital to understand these similarities and differences when choosing a model system to study a particular target, and critically, we provide a resource to do this. From a discovery perspective, studies performed in vitro in mouse neuronal cultures likely remain a valid and reliable option for researchers as the families of ion channels, GPCRs, and RKs are well conserved from mice to humans (Supplementary file 1, sheets 12–15, available at <http://links.lww.com/PAIN/A983>).

Our study has several limitations to acknowledge. The first is the choice of time point for the cultured DRG RNA-seq studies.

We chose 4 DIV for our studies. Given the literature on biochemical and  $\text{Ca}^{2+}$  imaging studies (which is too extensive to cite) we think that our findings will provide a substantial resource for studies of this nature as most of them are performed between 3 and 7 DIV. This can also be said for many electrophysiological studies on human DRG neurons as most investigators do experiments on these neurons over many days, with 4 DIV falling in the middle of the experimental spectrum for this small, but growing, body of work. The exception is mouse DRG electrophysiology where the vast majority of this very large literature has been performed at 24 hours after culturing. It is possible that some of the changes we observe at 4 DIV are not present at less than 1 DIV and/or that other differences are observed at this early time point. Another limitation is that changes in mRNA expression in culture may not represent differences in functional protein because some of these proteins may have long half-lives. In such a scenario, a downregulation of mRNA would not lead to any difference in functional protein over the time course of our experiment (4 DIV). This can only be addressed with proteomic or physiological<sup>53,76</sup> methods, which we have not performed. Finally, we have relied on bulk RNA sequencing in the work described here. We acknowledge that single cell sequencing would yield additional insights that will be useful for the field. This will be a goal of future work.

We have focused on using DRG from uninjured mice. Many studies have demonstrated that cultured DRG neurons from mice with neuropathic pain retain some neuropathic qualities in vitro, in particular spontaneous activity in a subpopulation of nociceptors.<sup>2,36,43,68,70</sup> This also occurs in human DRG neurons taken from people with neuropathic pain.<sup>43</sup> Our transcriptomic studies suggest that cultured DRG neurons from normal mice and human organ donors show some transcriptomic changes consistent with a neuropathic phenotype, but these neurons likely do not generate spontaneous activity. Some transcriptomic changes were found in mice but not conserved in humans, especially relevant for translational pharmacological studies in cultured mouse DRG. An example is caspase 6 (*Casp6*) which has been implicated in many neuropathic pain models in mice.<sup>5,6,36</sup> This gene was over 3-fold increased in mouse DRG culture but unchanged in human DRG cultures.

An interesting observation emerging from our work is that some macrophages are apparently present in DRG cultures and this macrophage phenotype is inflammatory in nature. An emerging literature describes DRG resident macrophages as key players in development of many chronic pain states, including neuropathic pain.<sup>24,28,43,54,66</sup> In future studies, it may be possible to manipulate these macrophages to interact with DRG neurons in culture to push this neuropathic pain phenotype further toward the generation of spontaneous activity. Such studies could allow for the generation of a neuropathic pain model in vitro. Such an advance would be particularly useful for the human organ donor DRG model, especially considering that neuropathic pain in patients is associated with a macrophage transcriptomic signature, at least in males.<sup>43</sup>

We have comprehensively characterized transcriptomic changes between native and cultured mouse and human DRG. These tissues are similar between the 2 species, suggesting that discovery work that is largely performed in mice faithfully models many physiological characteristics of human DRG neurons. There are, however, important differences between species and between native and cultured conditions, with minimal impact of the type of culturing protocol used. Our resource brings these differences to light. *A priori* knowledge of gene expression levels of a potential pharmacological or perturbation assay target in

mouse and human cultured and excised DRG can provide a convenient framework for the pain biologist to decide appropriate model system choice and delineate pharmacological divergences. Additional whole transcriptome assays at varying time points in culture, from different DRG culture protocols, in additional species, and subject to various perturbations (including sorted cell type specific cell-pools) can be integrated into our database to get a more comprehensive picture of the RNA landscape of mammalian DRG cultures.

## Conflict of interest statement

The authors have no conflicts of interest to declare.

## Acknowledgments

NIH grants T32DA007261 (L.A.M.); NS113457 (C.P.); NS065926 and NS102161 (T.J.P.); NS106953 and NS042595 (R.W.G.). Author contributions: conceived of the project: P.R. Ray, R.W. Gereau, and T.J. Price. Performed experiments: A. Wangzhou, L.A. McIlvried, C. Paige, P. Barragan-Iglesias, A. Ahmad, and S. Shiers. Supervised experiments: G. Dussor, R.W. Gereau, and T.J. Price. Analyzed data: A. Wangzhou, L.A. McIlvried, C. Paige, C.A. Guzman, and P.R. Ray. Supervised bioinformatics analysis: P.R. Ray. Drew figures: A. Wangzhou, A. Ahmad, S. Shiers, and P.R. Ray. Wrote and edited manuscript: A. Wangzhou, L.A. McIlvried, C. Paige, A. Ahmad, S. Shiers, G. Dussor, P.R. Ray, R.W. Gereau, and T.J. Price. All authors approved the final version of the manuscript.

## Appendix A. Supplemental digital content

Supplemental digital content associated with this article can be found online at <http://links.lww.com/PAIN/A983>.

## Article history:

Received 13 September 2019

Received in revised form 3 March 2020

Accepted 5 March 2020

Available online 17 March 2020

## References

- [1] Abbadie C, Bhangoo S, De Koninck Y, Malcangio M, Melik-Parsadaniantz S, White FA. Chemokines and pain mechanisms. *Brain Res Rev* 2009;60:125–34.
- [2] Amir R, Kocsis JD, Devor M. Multiple interacting sites of ectopic spike electrogenesis in primary sensory neurons. *J Neurosci* 2005;25:2576–85.
- [3] Basbaum AI, Bautista DM, Scherrer G, Julius D. Cellular and molecular mechanisms of pain. *Cell* 2009;139:267–84.
- [4] Benjamini H, Hochberg Y. Controlling the false discovery rate: a practical and powerful approach to multiple testing. *J Roy Stat Soc B* 1995;57:289–300.
- [5] Berta T, Park CK, Xu ZZ, Xie RG, Liu T, Lu N, Liu YC, Ji RR. Extracellular caspase-6 drives murine inflammatory pain via microglial TNF-alpha secretion. *J Clin Invest* 2014;124:1173–86.
- [6] Berta T, Perrin FE, Pertin M, Tonello R, Liu YC, Chamessian A, Kato AC, Ji RR, Decosterd I. Gene expression profiling of cutaneous injured and non-injured nociceptors in SNI animal model of neuropathic pain. *Sci Rep* 2017;7:9367.
- [7] Bhattacharjee A. On a measure of divergence between two statistical populations defined by their probability distributions. *Bull Cal Math Soc* 1943;35:99–109.
- [8] Bhave G, Karim F, Carlton SM, Gereau RW. Peripheral group I metabotropic glutamate receptors modulate nociception in mice. *Nat Neurosci* 2001;4:417–23.
- [9] Campbell JN, Meyer RA. Mechanisms of neuropathic pain. *Neuron* 2006;52:77–92.

- [10] Carlton SM. Localization of CaMKIIalpha in rat primary sensory neurons: increase in inflammation. *Brain Res* 2002;947:252–9.
- [11] Chen Y, Yang C, Wang ZJ. Ca<sup>2+</sup>/calmodulin-dependent protein kinase II alpha is required for the initiation and maintenance of opioid-induced hyperalgesia. *J Neurosci* 2010;30:38–46.
- [12] Chisolm DA, Cheng W, Colburn SA, Silva-Sanchez A, Meza-Perez S, Randall TD, Weinmann AS. Defining genetic variation in widely used congenic and backcrossed mouse models reveals varied regulation of genes important for immune responses. *Immunity* 2019;51:155–68 e155.
- [13] Chistiakov DA, Killingsworth MC, Myasoedova VA, Orekhov AN, Bobryshev YV. CD68/macrosialin: not just a histochemical marker. *Lab Invest* 2017;97:4–13.
- [14] Colbran RJ, Brown AM. Calcium/calmodulin-dependent protein kinase II and synaptic plasticity. *Curr Opin Neurobiol* 2004;14:318–27.
- [15] Conte C, Ebeling M, Marcuz A, Nef P, Andres-Barquin PJ. Evolutionary relationships of the Tas2r receptor gene families in mouse and human. *Physiol Genomics* 2003;14:73–82.
- [16] Davidson S, Golden JP, Copits BA, Ray PR, Vogt SK, Valtcheva MV, Schmidt RE, Ghetti A, Price TJ, Gereau RW. Group II mGluRs suppress hyperexcitability in mouse and human nociceptors. *PAIN* 2016;157:2081–8.
- [17] Davis AP, Grondin CJ, Johnson RJ, Sciaky D, McMorran R, Wieggers J, Wieggers TC, Mattingly CJ. The comparative toxicogenomics database: update 2019. *Nucleic Acids Res* 2019;47:D948–54.
- [18] Dobin A, Davis CA, Schlesinger F, Drenkow J, Zaleski C, Jha S, Batut P, Chaisson M, Gingeras TR. STAR: ultrafast universal RNA-seq aligner. *Bioinformatics* 2013;29:15–21.
- [19] Dussor GO, Price TJ, Flores CM. Activating transcription factor 3 mRNA is upregulated in primary cultures of trigeminal ganglion neurons. *Brain Res Mol Brain Res* 2003;118:156–9.
- [20] Eyre TA, Ducluzeau F, Sneddon TP, Povey S, Bruford EA, Lush MJ. The HUGO gene nomenclature database, 2006 updates. *Nucleic Acids Res* 2006;34:D319–321.
- [21] Ferrari LF, Bogen O, Levine JD. Role of nociceptor alphaCaMKII in transition from acute to chronic pain (hyperalgesic priming) in male and female rats. *J Neurosci* 2013;33:11002–11.
- [22] Frankish A, Diekhans M, Ferreira AM, Johnson R, Jungreis I, Loveland J, Mudge JM, Sisu C, Wright J, Armstrong J, Barnes I, Berry A, Bignell A, Carbonell Sala S, Chrast J, Cunningham F, Di Domenico T, Donaldson S, Fiddes IT, Garcia Giron C, Gonzalez JM, Grego T, Hardy M, Hourlier T, Hunt T, Izuogu OG, Lagarde J, Martin FJ, Martinez L, Mohanan S, Muir P, Navarro FCP, Parker A, Pei B, Pozo F, Ruffier M, Schmitt BM, Stapleton E, Suner MM, Sycheva I, Uszczynska-Ratajczak B, Xu J, Yates A, Zerbinio D, Zhang Y, Aken B, Choudhary JS, Gerstein M, Guigo R, Hubbard TJP, Kellis M, Paten B, Raymond A, Tress ML, Flicek P. GENCODE reference annotation for the human and mouse genomes. *Nucleic Acids Res* 2019;47:D766–73.
- [23] Goswami SC, Thierry-Mieg D, Thierry-Mieg J, Mishra S, Hoon MA, Mannes AJ, Iadarola MJ. Itch-associated peptides: RNA-Seq and bioinformatic analysis of natriuretic precursor peptide B and gastrin releasing peptide in dorsal root and trigeminal ganglia, and the spinal cord. *Mol Pain* 2014;10:44.
- [24] Hamidzadeh K, Christensen SM, Dalby E, Chandrasekaran P, Mosser DM. Macrophages and the recovery from acute and chronic inflammation. *Annu Rev Physiol* 2017;79:567–92.
- [25] Herrero J, Muffato M, Beal K, Fitzgerald S, Gordon L, Pignatelli M, Vilella AJ, Searle SM, Amode R, Brent S, Spooner W, Kulesha E, Yates A, Flicek P. Ensembl comparative genomics resources. *Database (Oxford)* 2016: bav096.
- [26] Hirai T, Mulpuri Y, Cheng Y, Xia Z, Li W, Ruangsri S, Spigelman I, Nishimura I. Aberrant plasticity of peripheral sensory axons in a painful neuropathy. *Sci Rep* 2017;7:3407.
- [27] Hu G, Huang K, Hu Y, Du G, Xue Z, Zhu X, Fan G. Single-cell RNA-seq reveals distinct injury responses in different types of DRG sensory neurons. *Sci Rep* 2016;6:31851.
- [28] Ji RR, Chamesian A, Zhang YQ. Pain regulation by non-neuronal cells and inflammation. *Science* 2016;354:572–7.
- [29] Ji RR, Xu ZZ, Wang X, Lo EH. Matrix metalloprotease regulation of neuropathic pain. *Trends Pharmacol Sci* 2009;30:336–40.
- [30] Kiguchi N, Maeda T, Kobayashi Y, Fukazawa Y, Kishioka S. Macrophage inflammatory protein-1alpha mediates the development of neuropathic pain following peripheral nerve injury through interleukin-1beta up-regulation. *PAIN* 2010;149:305–15.
- [31] Kuo D, Ding J, Cohn IS, Zhang F, Wei K, Rao DA, Roza C, Sokhi UK, Shanaj S, Oliver DJ, Echeverria AP, DiCarlo EF, Brenner MB, Bykerk VP, Goodman SM, Raychaudhuri S, Ratsch G, Ivashkiv LB, Donlin LT, HBEGF(+) macrophages in rheumatoid arthritis induce fibroblast invasiveness. *Sci Transl Med* 2019;11:eaau8587.
- [32] Liang Z, Hore Z, Harley P, Stanley FU, Michrowska A, Dahiya M, La Russa F, Jager SE, Villa-Hernandez S, Denk F. A transcriptional toolbox for exploring peripheral neuro-immune interactions. *bioRxiv* 2019:813980.
- [33] Lindborg JA, Niemi JP, Howarth MA, Liu KW, Moore CZ, Mahajan D, Zigmund RE. Molecular and cellular identification of the immune response in peripheral ganglia following nerve injury. *J Neuroinflammation* 2018;15: 192.
- [34] Lopes DM, Malek N, Edey M, Jager SB, McMurray S, McMahon SB, Denk F. Sex differences in peripheral not central immune responses to pain-inducing injury. *Sci Rep* 2017;7:16460.
- [35] Manning G, Whyte DB, Martinez R, Hunter T, Sudarsanam S. The protein kinase complement of the human genome. *Science* 2002;298:1912–34.
- [36] Megat S, Ray PR, Moy JK, Lou TF, Barragan-Iglesias P, Li Y, Pradhan G, Wangzhou A, Ahmad A, Burton MD, North RY, Dougherty PM, Khoutorsky A, Sonenberg N, Webster KR, Dussor G, Campbell ZT, Price TJ. Nociceptor translational profiling reveals the regulator-rag GTPase complex as a critical generator of neuropathic pain. *J Neurosci* 2019;39:393–411.
- [37] Megat S, Shiers S, Moy JK, Barragan-Iglesias P, Pradhan G, Seal RP, Dussor G, Price TJ. A critical role for dopamine D5 receptors in pain chronicity in male mice. *J Neurosci* 2018;38:379–97.
- [38] Melli G, Hoke A. Dorsal root ganglia sensory neuronal cultures: a tool for drug discovery for peripheral neuropathies. *Expert Opin Drug Discov* 2009;4:1035–45.
- [39] Mickle AD, Gereau RW. A bright future? Optogenetics in the periphery for pain research and therapy. *PAIN* 2018;159(suppl 1):S65–73.
- [40] Nguyen MQ, Le Pichon CE, Ryba N. Stereotyped transcriptomic transformation of somatosensory neurons in response to injury. *Elife* 2019;8:e49679.
- [41] Nichio BTL, Marchaukoski JN, Raittz RT. New tools in orthology analysis: a brief review of promising perspectives. *Front Genet* 2017;8:165.
- [42] Niemi JP, DeFrancesco-Lisowitz A, Roldan-Hernandez L, Lindborg JA, Mandell D, Zigmund RE. A critical role for macrophages near axotomized neuronal cell bodies in stimulating nerve regeneration. *J Neurosci* 2013; 33:16236–48.
- [43] North RY, Li Y, Ray P, Rhines LD, Tatsui CE, Rao G, Johansson CA, Zhang H, Kim YH, Zhang B, Dussor G, Kim TH, Price TJ, Dougherty PM. Electrophysiological and transcriptomic correlates of neuropathic pain in human dorsal root ganglion neurons. *Brain* 2019;142:1215–26.
- [44] Ono K, Xu S, Hitomi S, Inenaga K. Comparison of the electrophysiological and immunohistochemical properties of acutely dissociated and 1-day cultured rat trigeminal ganglion neurons. *Neurosci Lett* 2012;523:162–6.
- [45] Parisien M, Khoury S, Chabot-Dore AJ, Sotocinal SG, Slade GD, Smith SB, Fillingim RB, Ohrbach R, Greenspan JD, Maixner W, Mogil JS, Belfer I, Diatchenko L. Effect of human genetic variability on gene expression in dorsal root ganglia and association with pain phenotypes. *Cell Rep* 2017; 19:1940–52.
- [46] Pearson K. Notes on regression and inheritance in the case of two parents. *Proc R Soc Lond* 1895;58:240–2.
- [47] Perry RB, Hezroni H, Goldrich MJ, Ulitsky I. Regulation of neuroregeneration by long noncoding RNAs. *Mol Cell* 2018;72:553–67 e555.
- [48] Perteau M, Perteau GM, Antonescu CM, Chang TC, Mendell JT, Salzberg SL. StringTie enables improved reconstruction of a transcriptome from RNA-seq reads. *Nat Biotechnol* 2015;33:290–5.
- [49] Pimentel H, Bray NL, Puente S, Melsted P, Pachter L. Differential analysis of RNA-seq incorporating quantification uncertainty. *Nat Methods* 2017; 14:687–90.
- [50] Price TJ, Gold MS. From mechanism to cure: renewing the goal to eliminate the disease of pain. *Pain Med* 2018;19:1525–49.
- [51] Ray P, Torck A, Quigley L, Wangzhou A, Neiman M, Rao C, Lam T, Kim JY, Kim TH, Zhang MQ, Dussor G, Price TJ. Comparative transcriptome profiling of the human and mouse dorsal root ganglia: an RNA-seq-based resource for pain and sensory neuroscience research. *PAIN* 2018;159: 1325–45.
- [52] Rouillard AD, Gundersen GW, Fernandez NF, Wang Z, Monteiro CD, McDermott MG, Ma'ayan A. The harmonizome: a collection of processed datasets gathered to serve and mine knowledge about genes and proteins. *Database (Oxford)* 2016:baw100.
- [53] Sheahan TD, Valtcheva MV, Mcllvried LA, Pullen MY, Baranger DAA, Gereau RW. Metabotropic glutamate receptor 2/3 (mGluR2/3) activation suppresses TRPV1 sensitization in mouse, but not human, sensory neurons. *eNeuro* 2018;5:ENEURO.0412-17.2018.
- [54] Shepherd AJ, Copits BA, Mickle AD, Karlsson P, Kadunganattil S, Haroutounian S, Tadinada SM, de Kloet AD, Valtcheva MV, Mcllvried LA, Sheahan TD, Jain S, Ray PR, Usachev YM, Dussor G, Krause EG, Price

- TJ, Gereau RW, Mohapatra DP. Angiotensin II triggers peripheral macrophage-to-sensory neuron redox crosstalk to elicit pain. *J Neurosci* 2018;38:7032–57.
- [55] Stone LS, Molliver DC. In search of analgesia: emerging roles of GPCRs in pain. *Mol Interv* 2009;9:234–51.
- [56] Student. The probable error of a mean. *Biometrika* 1908;6:1–25.
- [57] Thakur M, Crow M, Richards N, Davey GI, Levine E, Kelleher JH, Agle CC, Denk F, Harridge SD, McMahon SB. Defining the nociceptor transcriptome. *Front Mol Neurosci* 2014;7:87.
- [58] The Gene Ontology C. The Gene Ontology Resource: 20 years and still GOing strong. *Nucleic Acids Res* 2019;47:D330–8.
- [59] Tillu DV, Hassler SN, Burgos-Vega CC, Quinn TL, Sorge RE, Dussor G, Boitano S, Vagner J, Price TJ. Protease-activated receptor 2 activation is sufficient to induce the transition to a chronic pain state. *PAIN* 2015;156:859–67.
- [60] Turk R, t Hoen PA, Sterrenburg E, de Menezes RX, de Meijer EJ, Boer JM, van Ommen GJ, den Dunnen JT. Gene expression variation between mouse inbred strains. *BMC Genomics* 2004;5:57.
- [61] Usoskin D, Furlan A, Islam S, Abdo H, Lonnerberg P, Lou D, Hjerling-Leffler J, Haeggstrom J, Kharchenko O, Kharchenko PV, Linnarsson S, Ernfors P. Unbiased classification of sensory neuron types by large-scale single-cell RNA sequencing. *Nat Neurosci* 2015;18:145–53.
- [62] Valtcheva MV, Copits BA, Davidson S, Sheahan TD, Pullen MY, McCall JG, Dikranian K, Gereau RW. Surgical extraction of human dorsal root ganglia from organ donors and preparation of primary sensory neuron cultures. *Nat Protoc* 2016;11:1877–88.
- [63] Vergnolle N, Bunnett NW, Sharkey KA, Brussee V, Compton SJ, Grady EF, Cirino G, Gerard N, Basbaum AI, Andrade-Gordon P, Hollenberg MD, Wallace JL. Proteinase-activated receptor-2 and hyperalgesia: a novel pain pathway. *Nat Med* 2001;7:821–6.
- [64] Wallace TL, Johnson EM Jr. Cytosine arabinoside kills postmitotic neurons: evidence that deoxycytidine may have a role in neuronal survival that is independent of DNA synthesis. *J Neurosci* 1989;9:115–24.
- [65] Wang F, Flanagan J, Su N, Wang LC, Bui S, Nielson A, Wu X, Vo HT, Ma XJ, Luo Y. RNAscope: a novel in situ RNA analysis platform for formalin-fixed, paraffin-embedded tissues. *J Mol Diagn* 2012;14:22–9.
- [66] Watkins LR, Maier SF. Beyond neurons: evidence that immune and glial cells contribute to pathological pain states. *Physiol Rev* 2002;82:981–1011.
- [67] Woolf CJ, Ma Q. Nociceptors—noxious stimulus detectors. *Neuron* 2007;55:353–64.
- [68] Wu Z, Li L, Xie F, Du J, Zuo Y, Frost JA, Carlton SM, Walters ET, Yang Q. Activation of KCNQ channels suppresses spontaneous activity in dorsal root ganglion neurons and reduces chronic pain after spinal cord injury. *J Neurotrauma* 2017;34:1260–70.
- [69] Yang DP, Zhang DP, Mak KS, Bonder DE, Pomeroy SL, Kim HA. Schwann cell proliferation during Wallerian degeneration is not necessary for regeneration and remyelination of the peripheral nerves: axon-dependent removal of newly generated Schwann cells by apoptosis. *Mol Cell Neurosci* 2008;38:80–8.
- [70] Yang Q, Wu Z, Hadden JK, Odem MA, Zuo Y, Crook RJ, Frost JA, Walters ET. Persistent pain after spinal cord injury is maintained by primary afferent activity. *J Neurosci* 2014;34:10765–9.
- [71] Yarwood RE, Imlach WL, Lieu T, Veldhuis NA, Jensen DD, Klein Herenbrink C, Aurelio L, Cai Z, Christie MJ, Poole DP, Porter CJH, McLean P, Hicks GA, Geppetti P, Halls ML, Canals M, Bunnett NW. Endosomal signaling of the receptor for calcitonin gene-related peptide mediates pain transmission. *Proc Natl Acad Sci U S A* 2017;114:12309–14.
- [72] Young JM, Friedman C, Williams EM, Ross JA, Tonnes-Priddy L, Trask BJ. Different evolutionary processes shaped the mouse and human olfactory receptor gene families. *Hum Mol Genet* 2002;11:535–46.
- [73] Yu X, Liu H, Hamel KA, Morvan MG, Yu S, Leff J, Guan Z, Braz JM, Basbaum AI. Dorsal root ganglion macrophages contribute to both the initiation and persistence of neuropathic pain. *Nat Commun* 2020;11:264.
- [74] Yu Y, Huang X, Di Y, Qu L, Fan N. Effect of CXCL12/CXCR4 signaling on neuropathic pain after chronic compression of dorsal root ganglion. *Sci Rep* 2017;7:5707.
- [75] Zeisel A, Hochgerner H, Lonnerberg P, Johnsson A, Memic F, van der Zwan J, Haring M, Braun E, Borm LE, La Manno G, Codeluppi S, Furlan A, Lee K, Skene N, Harris KD, Hjerling-Leffler J, Arenas E, Ernfors P, Marklund U, Linnarsson S. Molecular architecture of the mouse nervous system. *Cell* 2018;174:999–1014.e1022.
- [76] Zhang X, Priest BT, Belfer I, Gold MS. Voltage-gated Na(+) currents in human dorsal root ganglion neurons. *Elife* 2017;6:e23235.
- [77] Zhang XD, Marine SD, Ferrer M. Error rates and powers in genome-scale RNAi screens. *J Biomol Screen* 2009;14:230–8.